The Active-Site [4Fe-4S] Cluster in the Isoprenoid Biosynthesis Enzyme IspH Adopts Unexpected Redox States during Ligand Binding and Catalysis

Selamawit Ghebreamlak, Sebastian A. Stoian,* Nicholas S. Lees, Bryan Cronin, Forrest Smith, Matthew O. Ross, Joshua Telser, Brian M. Hoffman, and Evert C. Duin*

ABSTRACT: (*E*)-4-Hydroxy-3-methylbut-2-enyl diphosphate reductase, or IspH (formerly known as LytB), catalyzes the terminal step of the bacterial methylerythritol phosphate (MEP) pathway for isoprene synthesis. This step converts (*E*)-4-hydroxy-3-methylbut-2-enyl diphosphate (HMBPP) into one of two possible isomeric products, either isopentenyl diphosphate (IPP) or dimethylallyl diphosphate (DMAPP). This reaction involves the removal of the C4 hydroxyl group of HMBPP and addition of two electrons. IspH contains a [4Fe-4S] cluster in its active site, and multiple cluster-based paramagnetic species of uncertain redox and ligation states can be detected after incubation with reductant, addition of a ligand, or during catalysis. To characterize the clusters in these species, ^{57}Fe-labeled samples of IspH were prepared and studied by electron paramagnetic resonance (EPR), ^{57}Fe electron−nuclear double resonance (ENDOR), and Mössbauer spectroscopies. Notably, this ENDOR study provides a rarely reported, complete determination of the ^{57}Fe hyperfine tensors for all four Fe ions in a [4Fe-4S] cluster. The resting state of the enzyme (Ox) has a diamagnetic $[4Fe\text{-}4S]^{2+}$ cluster. Reduction generates $[4Fe\text{-}4S]^{+}$ (Red) with both $S = 1/2$ and $S = 3/2$ spin ground states. When the reduced enzyme is incubated with substrate, a transient paramagnetic reaction intermediate is detected (Int) which is thought to contain a cluster-bound substrate-derived species. The EPR properties of Int are indicative of a 3+ iron−sulfur cluster oxidation state, and the Mössbauer spectra presented here confirm this. Incubation of reduced enzyme with the product IPP induced yet another paramagnetic $[4Fe\text{-}4S]^{+}$ species (Red+P) with $S = 1/2$. However, the g-tensor of this state is commonly associated with a 3+ oxidation state, while Mössbauer parameters show features typical for 2+ clusters. Implications of these complicated results are discussed.

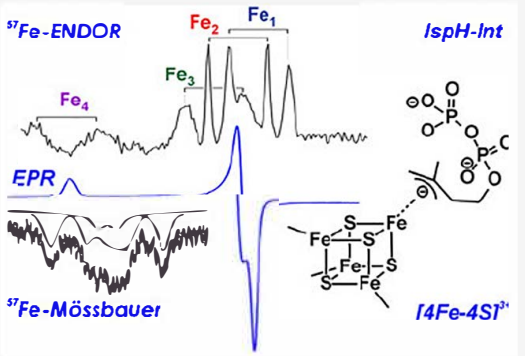

In this paper we provide new insight into the electronic and magnetic properties of the active site [4Fe-4S] cluster in (*E*)-4-hydroxy-3-methylbut-2-enyl diphosphate reductase or IspH (formerly known as LytB). These results are of importance, as the enzyme is a target for drug development. The results support the proposed organometallic type reaction mechanism and highlight unique properties of the [4Fe-4S] cluster which is directly involved in substrate binding and catalysis. There are only a few types of 4Fe cluster-containing enzymes known that do a similar type of catalysis, but this family appears to be growing, and here we provide both simple and more advanced spectroscopic methods to quickly recognize these types of enzymes.[1−6]

IspH catalyzes the terminal step of the bacterial methylerythritol phosphate (MEP) pathway for isoprene synthesis.[7] This pathway is utilized exclusively by a group of eubacteria and apicomplexan parasites,[8] so development of inhibitors for the MEP pathway could result in treatment, for example, for malaria, tuberculosis (TB), anthrax, plague, cholera, venereal diseases, and enteric infections.[9−15] Isoprenoid synthesis in humans proceeds via the Mevalonate pathway and is therefore unlikely to be affected by drugs that target the MEP pathway. Such drug development requires a full understanding of the enzyme properties and mechanism.

IspH converts (*E*)-4-hydroxy-3-methylbut-2-enyl diphosphate (HMBPP) into one of two possible isomeric products, either isopentenyl diphosphate (IPP) or dimethylallyl diphosphate (DMAPP) in a ratio of 5:1 (Figure 1).[7] This reaction involves the removal of the C4 hydroxyl group of HMBPP and addition of two electrons. The [4Fe-4S] cluster is essential for this process. Three of the Fe ions in the cluster are

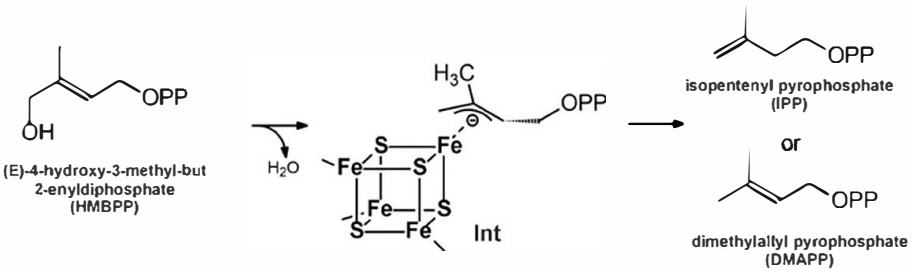

Figure 1. Reaction catalyzed by IspH and the proposed $[4Fe\text{-}4S]^{3+}$–allyl anion/η^3 intermediate (Int) formed during the reaction mechanism.

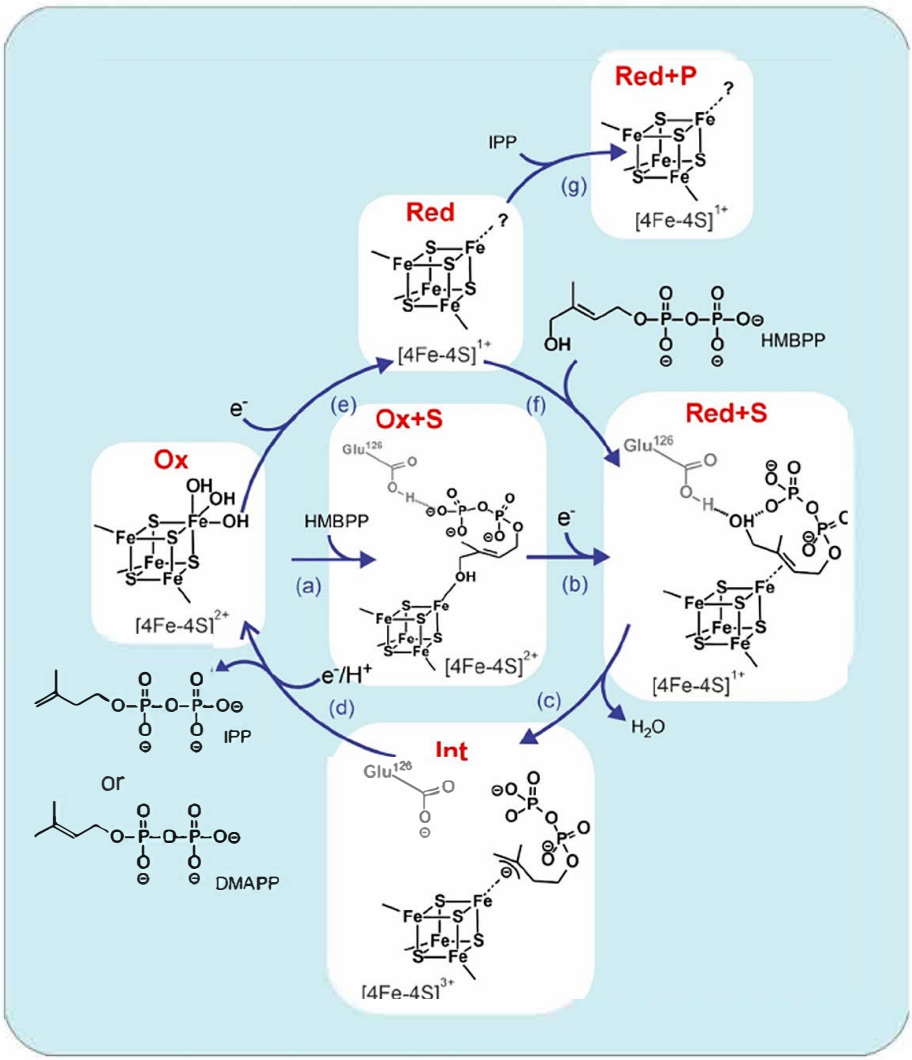

Figure 2. Proposed structures for different states of IspH observed during different reaction conditions. IspH has a unique (atypical) iron that in the Ox state ($[4Fe\text{-}4S]^{2+}$) has an octahedral geometry with a first coordination sphere consisting of three sulfur atoms (inorganic sulfides) and three oxygen atoms from three water or hydroxide molecules/ions.[32] The cysteinyl ligands to each of the other (typical) iron sites are indicated by lines. In the proposed organometallic model for the reaction of IspH with HMBPP, the substrate binds via its hydroxyl group to the Ox state forming the Ox+S state (step a). Upon reduction of the cluster, a π- or η^2-complex is formed, and the hydroxyl group swings away from the cluster forming the Red+S state (step b). Proximity of the hydroxyl group to a Glu residue (E126) in the active site allows protonation of its hydroxyl group and release as a water molecule, forming the reaction intermediate species Int (step c). The transfer of an additional electron from an external source is needed for the reaction to go to completeness and form IPP and DMAPP (step d). In the studies described here the Red state is first formed by the addition of dithionite (step e); this is then reacted with HMBPP and produces the same reaction intermediate species Int, presumably via the Red+S form (steps f and c) but that species was not observed and might be too short-lived. It is also possible to add IPP to the Red form inducing a different species: Red+P (step g). The cluster coordination sphere in the different states is based on ^{2}H-, ^{31}P-, ^{13}C-, and ^{17}O-labeling studies.[5,16–19,34] It is not clear what non-Cys ligand(s) (if any) is present in the Red state. In this state IPP might bind to the cluster in a similar way as HMBPP in the Red+S state but there is no evidence available for this. The assignment of the oxidation states for the [4Fe-4S] clusters, in particular the Int and Red+P states, is discussed in the text.

coordinated by a Cys residue, while the fourth—the unique Fe—is not. It was discovered that a reaction intermediate directly coordinates to the unique Fe during the reaction mechanism. The structure of the intermediate, denoted "Int" in Figure 2, is based on ^{2}H-, ^{31}P-, ^{13}C-, and ^{17}O- electron–nuclear double resonance (ENDOR) and hyperfine sublevel correlation (HYSCORE) studies and X-ray crystallographic data.[16−19]

The canonical [4Fe-4S] clusters can be divided into two varieties, a low potential (ferredoxin, Fd) type that switches between the 1+ and 2+ oxidation states and a high potential type (high potential iron sulfur protein, HiPIP) that switches between the 2+ and 3+ oxidation states.[20] In both cases, the cluster can transfer or store only one electron at-a-time during oxidative switching. During catalysis the electrons are typically donated to the cluster from an outside donor[21] and passed one by one to the substrate. Therefore, it was expected that a radical species might be generated during the reduction of HMBPP by IspH, but instead a species denoted "**Int**" is formed that displays a cluster-based electron paramagnetic resonance (EPR) signal.[16] The shape and temperature behavior of this signal is completely different from that of the two canonical varieties (1+ and 3+ forms), which both can be detected without power saturation in the 6 to 20 K range, and become unobservable as the temperature is increased.[22−24] Instead the signal of **Int** is detectable up to 100 K. The behavior and shape of the **Int** signal resemble those of a species detected in ferredoxin:thioredoxin reductase (Ftr, EC 1.8.7.2).[25−28] Ftr uses single electrons donated by ferredoxin for a two-electron reduction of a disulfide bond between two Cys residues present on the substrate thioredoxin. The active site of Ftr also contains a pair of Cys residues in close proximity to the [4Fe-4S] cluster. Ftr transfers two electrons to the disulfide and the unique Fe binds one of the cysteine sulfurs forming a coordination sphere consisting of two cysteinates and three sulfides. Mössbauer data for this species showed that the resulting cluster has a 3+ oxidation state.[28] Despite the differences in the types of reaction catalyzed by IspH and Ftr, based on the highly similar properties of the respective EPR signals, our group has supported the assignment of 3+ oxidation for the [4Fe-4S] cluster in the **Int** state, but assignments of 1+ and even 2+ (surprisingly, given the cluster spin of 1/2) can also be found.[16,29−31]

Although several versions of the catalytic cycle for the conversion of HMBP by IspH have been proposed,[16,29−31] we support the organometallic model shown in Figure 2, where we have assigned new names (**Ox**, **Ox+S**, **Red**, **Red+S**, **Red+P**, and **Int**) to each state to facilitate discussion of the results presented here and described in the literature. Nuclear Resonance Vibrational Spectroscopy (NRVS) measurements indicated that in the "resting" **Ox** state ($[4Fe\text{-}4S]^{2+}$), the unique iron has an octahedral geometry with a first coordination sphere consisting of three sulfur atoms (cluster sulfide ions, as expected) and three oxygen atoms from three water or hydroxyl ligands—a previously unknown coordination sphere for an FeS cluster.[32] HMBPP first binds to the cluster in the **Ox** state of the enzyme via the hydroxyl group: **Ox+S** (step a).[19] This state might be skipped when substrate is added to reduced enzyme (steps e and f) since upon reduction the substrate, a π- or η^2-complex is formed and the hydroxyl group swings away from the cluster **Red+S** (step b).[19]

The **Red+S** form has not been directly observed, but X-ray crystallographic studies indicated the possible formation of such a reaction intermediate[28] and kinetic studies also support such a model.[33] Additional evidence came from studies of an IspH variant, E126Q, in which a key glutamate residue (shown in Figure 2) is rendered inactive by mutation to glutamine,[17] which presumably prevents removal of the hydroxyl group. A paramagnetic species accumulates in the E126Q variant characterized by g = [2.124, 1.999, 1.958] (g_{avg} = 2.027) and ^{13}C-ENDOR and HYSCORE data obtained with ^{13}C-labeled HMBPP was indicative for the formation of a π-complex.[18,34] A π-complex was first observed with the catalytic cofactor of nitrogenase,[35] and the feasibility of this type of bonding was recently proven in model compounds with alkyne and alkene adducts of synthetic $[4Fe\text{-}4S]^{+}$ clusters.[36] Theoretical support for the switch in binding mode of HMBPP comes from density functional theory/self-consistent reaction field (DFT/SCRF) computations that indicate that in the diamagnetic **Ox+S** form the lowest energy is for a state wherein the substrate coordinates the unique or atypical iron via an alcohol group (ROH).[37] Upon reduction of the cluster, however, the situation changes and η^2-bound states have lower energies than ROH-bound states.[38] The formation of this putative π- or η^2-complex **Red+S** inspired synthesis of a set of inhibitors that contained double and triple bonds. Several of these have K_I values as low as 245 to 0.45 μM.[39] The **Red+S** species is probably short-lived since the proximity of the hydroxyl group to a Glu residue in the active site allows protonation of its hydroxyl group and release as a water molecule (step c). We propose that this goes together with an internal transfer of two electrons to form the EPR-active **Int** reaction intermediate species with the [4Fe-4S] cluster now in the 3+ oxidation state. Studies with labeled HMBPP are in line with an η^3- or allyl anion model.[30,40] Lastly, the reaction intermediate **Int** needs the transfer of an additional electron from an external source to form either IPP or DMAPP (step d). In the cell, ferredoxins and flavodoxins have been proposed to be the natural electron donors,[41] while dithionite is employed in the rapid freeze-quench (RFQ) studies presented here. In Figure 2, we incorporate an additional state, **Red+P**, which can be generated by the addition of IPP to the **Red** form (step g). This species also appears in the RFQ studies due to the accumulation of the products IPP and DMAPP.

As this summary shows, the study of mechanism and intermediates in IspH catalysis/inhibition has unsurprisingly focused on the nature of substrate/inhibitor-derived species bound to the unique cluster Fe but the redox state of the **Int** and **Red+P** species was never determined. Here we show that the cluster in intermediate states in fact has unique properties that underlie catalysis by this enzyme. To explore these properties, ^{57}Fe-labeled samples of IspH were prepared and studied in the several forms of the catalytic cycle by 35 GHz ENDOR and Mössbauer spectroscopies. Previous ^{57}Fe-ENDOR studies of [4Fe-4S] clusters have either been carried out on single crystals of model clusters,[42,43] or have involved fitting of broad and highly overlapped signals from enzymic clusters, often recorded at X-band frequencies.[44,45] The 35 GHz ^{57}Fe ENDOR spectra collected here for uniformly labeled IspH states in frozen solution are of such exceptional resolution that 2D field-frequency plots of ENDOR spectra collected across the EPR envelopes have allowed the hyperfine tensors for all four iron atoms to be determined in the **Int** and **Red+P** IspH states.

MATERIALS AND METHODS

Chemicals. *E. coli* strain XL-1 blue was purchased from Agilent technology (Santa Clara, CA). IPP, DMAPP, and HMBPP (as a purity standard) were from Echelon biosciences (Salt Lake City, UT). Sodium dithionite was from Alfa Aesar (Haverhill, MA). All gases and gas mixtures were from Airgas (Radnor Township, PA). All other chemicals were from AMRESCO (Solon, OH), Acros/Thermo Fisher Scientific (New Jersey) or Sigma-Aldrich (St. Louis, MO). His-trap Ni^{2+} affinity and PD-10 columns were from Cytiva. Centricon and Amicon ultrafiltration units were from Millipore (Billerica, MA). Elemental ^{57}Fe (97−98%) was purchased from WEB Research (Edina, MN) or Cambridge Isotope Laboratories, Inc. (Tewksbury, MA). $^{57}FeCl_3$ was prepared by dissolving ^{57}Fe (solid) in 37% HCl at room temperature. After all iron was dissolved, 5 M NaOH was added to bring the $^{57}FeCl_3$ solution to a pH of 4−5. The stock solution was stored at 4 °C until use.

Purification steps, sample handling, and experiments were done in an anaerobic chamber (Coy Laboratory Products, Inc., Grass Lake, MI) filled with a mixture of 95% N_2 and 5% H_2 or a Vacuum Atmospheres Co. drybox filled with argon (Hawthorne, CA). Oxygen levels in the Coy chamber are typically in the 5−15 ppm range. Buffers and solutions free of molecular oxygen were used in all procedures. The buffers were filtered over a 0.45 μm membrane (Fisher Scientific Pittsburgh, PA) and subsequently brought to a boil while sparging the buffer with nitrogen gas. Subsequently, the buffers were stirred under vacuum for 2−3 h. The closed-off bottles were repressurized with nitrogen and directly used or stored. All buffers and solutions were equilibrated and stirred overnight inside the glovebox before use.

(*E*)-4-Hydroxy-3-methylbut-2-enyl Diphosphate (HMBPP) Synthesis. HMBPP, the substrate for IspH, was synthesized as described in the literature.[46,47] In the first step, (*E*)-4-chloro-2-methylbut-2-en-1-ol was synthesized: $TiCl_4$ (285 mg, 1.5 mmol, 164.5 μL) was dissolved in 3 mL of dry CH_2Cl_2 under argon and the solution was cooled to −80/−90 °C followed by dropwise addition, with stirring, of 84 mg of 2-methyl-2-vinyloxirane in 0.4 mL of dry CH_2Cl_2. The mixture was stirred for 90 min and the reaction was quenched with 5 mL 1 N HCl. When the mixture was warmed to room temperature the phases separated. The aqueous layer was extracted 4 times with 20 mL of diethyl ether and the combined organic phase was dried over $MgSO_4$. The organic extract was purified with flash chromatography (diethyl ether/hexane 1:1 v/v). Collected fractions were run on TLC (ethyl acetate/hexane 1:4 v/v) and stained with $KMnO_4$. Fractions that contain the desired product were collected and the solvent was removed to afford (*E*)-4-chloro-2-methylbut-2-en-1-ol. The purity of the product was confirmed with NMR spectroscopy. ^1H NMR (CD_3CN, 400 MHz): 5.62 (*tq*, J = 8.2; 1.58, 1H), 4.16 (*d*, J = 8.2, 2H), 3.89 (*s*, 2H), 1.64 (*d*, J = 1.60, 3H).

In the second step, tris(tetra-*n*-butylammonium) hydrogen pyrophosphate was synthesized: Disodium dihydrogen pyrophosphate (3.13 g, 14 mmol) was dissolved in 25 mL of deionized water containing 1 mL of concentrated NH_4OH. The clear solution was passed over a cation exchange resin Dowex 50WX8 (2 × 30 cm, H^+ form) and developed with deionized water. The first 150 mL fraction was collected and titrated with tetrabutylammonium hydroxide to a pH of 7.3. The fractions were lyophilized resulting in a flocculent white tris(tetra-*n*-butylammonium) hydrogen pyrophosphate.

In the final step, the two compounds from steps 1 and 2 were combined into HMBPP: Tris(tetra-*n*-butylammonium) hydrogen pyrophosphate (227 mg, 0.25 mmol) in 400 μL of MeCN was added slowly to 25 mg of (*E*)-4-chloro-2-methylbut-2-en-1-ol (0.21 mmol) in 250 μL of MeCN affording an orange-red solution. The solution was stirred for 2 h at room temperature and the solvent was removed under reduced pressure. The orange-colored oily residue was dissolved in 3 mL of H_2O and passed over a column of DOWEX 50WX8 (1 × 4 cm, NH_4^+ form) that has been prequilibrated with 20 mL of 25 mM NH_4HCO_3. The diphosphate was eluted with 20 mL of 25 mM NH_4HCO_3, flash frozen and lyophilized to yield tan colored (*E*)-1-hydroxy-2-methylbut-2-enyl-4-diphosphate (HMBPP). ^1H NMR (D_2O, 400 MHz): 5.52 (*tq*, J = 6.9, 1H), 4.39 (*t*, J = 7.2, 2H), 3.88 (*s*, 2H), 1.57 (*s*, 3H).

Expression and Purification. All enzymes are expressed in *E. coli*, but different genetic sources were used: *Plasmodium falciparum*, and *E. coli*. The reason for using IspH from different sources is that IspH from *P. falciparum* is more stable but contains low cluster content, while IspH from *E. coli* is less stable but has a higher cluster content. We also found that when making variant enzymes, successful folding could depend on which gene to use. As a result, the ENDOR data presented here are produced with *P. falciparum* IspH, while the Mössbauer data were produced with *E. coli* IspH. In earlier work we showed that the EPR spectra for the different paramagnetic states from either genetic source are very similar.[16]

The expression plasmid for IspH from *P. falciparum* was provided by the group of Dr. Hassam Jomaa at the Justus-Liebig University at Giessen, Germany.[7] The expression plasmid for WT IspH from *E. coli* was provided by the group of Dr. Michael Groll from the Technical University, Munich, Germany.[48] All IspH proteins contained a His_6-tag for purification by immobilized nickel affinity chromatography. Transformation of *E. coli* XL-1 blue cells with the respective plasmids was performed by heat shock of the cells at 42 °C for 45 s. The transformed cells were used to inoculate super optimal medium with catabolic repressor (SOC medium: 20 g tryptone, 5 g yeast extract, 0.5 g NaCl, 10 mL 1 M $MgSO_4$, 10 mL 1 M $MgCl_2$, 20% glucose, 100 mg ampicillin per liter) and grown at 37 °C for 2 h. Cells were put on Luria−Bertani (LB) agar plates containing ampicillin (100 mg/L) and incubated at 37 °C overnight. A 5 mL-cell culture in SOC medium was grown for 6 h at 37 °C under constant shaking (250 rpm). The 5 mL culture was used to inoculate 100 mL SOC medium which was supplemented with 50 μL 1 M $FeCl_3$ (for a ^{57}Fe-isotope-enriched protein, $^{57}FeCl_3$ was used) and allowed to grow overnight while shaking (250 rpm) at 37 °C. The 100 mL cultures could be used to make glycerol stocks to be stored at −80 °C or used for further culturing. From an overnight 100 mL culture, 50 mL was transferred to a 1 L diluted SOC medium containing 500 μL 1 M $FeCl_3$. For IspH from *P. falciparum*, anhydrotetracycline at a concentration of 1 mg/L was used as inducer. This was added at an OD_{600} of 0.3. No inducer was needed for the IspH from *E. coli*. The cultures were incubated until the OD_{600} reached 3−4.5 and were harvested by centrifugation at 3000 RCF for 20 min. Cell pellets were stored at −80 °C.

The cell pellet was resuspended in 100 mL 30 mM Tris-HCl, 100 mM NaCl, pH 8.0 (buffer A), and lysed by sonication (Branson Digital Sonifier 450), 3 times for 3 min each at 60% power, with a 0.5 s on/0.5 s off pulse on ice, followed by centrifugation at 126,603 RCF for 20 min at 4 °C (Beckman XL-70 Ultracentrifuge, TYPE 45 Ti Rotor, Beckman Coulter, Inc.). The cell extract was filtered with a 0.2 μm filter (Millipore) and loaded to a prewashed His-trap Ni^{2+} affinity column. The protein was eluted with an imidazole gradient (0% to 100%) in 30 mM Tris-HCl, 100 mM NaCl, 500 mM imidazole, pH 8.0 (buffer B). The enzyme eluted at about 10−15% buffer B. IspH fractions with a purity of 90−95%, ascertained by SDS-PAGE, were pooled, the imidazole was removed by washing with buffer A (using an Amicon protein concentrator or a Millipore Centricon centrifugal device with 10 kDa filters) and immediately used or stored at 4 °C.

Protein and Iron Determination. The protein concentration was determined with the Bradford assay[49] with bovine serum albumin as a standard or by measuring the absorbance at 280 nm using ε = 19,940 $M^{-1}cm^{-1}$ for *E. coli* IspH, and 41,260 $M^{-1}cm^{-1}$ for *P. falciparum* IspH. These were calculated using a protein extinction calculator (https://www.biomol.net/en/tools/proteinextinction.htm). A rapid ferrozine-based colorimetry assay was used to determine the iron content of the protein.[50] All containers and pipet tips were boiled in 1 M HCl and washed with ultrapure water before use. Iron standards (0, 10, 20, 30, 40, 50 μM) were prepared by dissolving ferrous ethylenediammonium sulfate in 10 mM HCl. The iron-releasing reagent was prepared by mixing equal volumes of 0.6 M HCl and 4.5% potassium permanganate. The iron chelating and reducing reagent contained 6.5 M ferrozine, 13.1 mM neocuprine, 2 M ascorbic acid, and 5 M ammonium acetate in a 25 mL solution. To

1 mL iron standard samples and the protein samples, 0.5 mL of the iron-releasing reagent was added, followed by incubation at 60 °C in a water-bath for 2 h. To each sample 100 μL of the iron chelating and reducing reagent was added followed by incubation for at least another 30 min. The absorbance at 562 nm was measured and the values of the samples and standards were compared to determine the iron concentration in the protein samples.

Steady-State Kinetic Analysis. A photometric assay was used to investigate the steady-state kinetics of IspH. To a solution of IspH (in 30 mM Tris-HCl, 100 mM NaCl, pH 8.0), sodium-dithionite-reduced methyl viologen (MV), and varied concentrations of HMBPP were added. The change in absorbance at 603 nm as a function of time was monitored. The assay was performed under anaerobic conditions with a temperature-controlled cuvette holder (q pod) inside a glovebox that was connected through fiber optics to an Agilent 8453 UV–visible spectrophotometer (Palo Alto, CA). All measurements were performed at 25 °C. The data were fit to the Michaelis–Menten equation using Origin software to obtain the steady-state kinetic parameters, which were calculated as the average of three separate experiments.

Rapid-Freeze-Quench (RFQ). The rapid-freeze-quench method was used to trap intermediates in the enzymatic reaction. An RQF-3 Quench-Flow Instrument (KinTek Corporation, Snow Shoe, PA, https://kintekcorp.com/) was used to rapidly mix and freeze samples. The RQF-3 was modified by KinTek to operate inside the Vacuum Atmospheres Co. drybox with an additional attachment piece to collect the frozen sample on the outside of the box. IspH in the presence of an excess sodium dithionite was loaded in one syringe and in the second syringe the HMBPP solution was loaded. Enzyme and substrate concentrations were set to a ratio of 1:10. The reaction mixture, a final volume of 300 μL, was aged at 25 °C and quenched at a predetermined period in cold isopentane. The "snow" was subsequently packed into an EPR tube. Samples for longer incubation time were mixed by hand and quenched with cold ethanol. Each sample was analyzed by EPR spectroscopy. There is a 30% difference in intensity in samples prepared by hand and samples prepared with the RFQ setup due to the empty space left in between the packed snow particles. The figures presented in this paper have all been corrected for this difference.

X-Band EPR Data Collection. CW EPR spectra were collected at X-band frequency with a Bruker EMX spectrometer (Bruker Biospin Corporation, Billerica, MA) fitted with the ER-4119-HS high sensitivity perpendicular-mode cavity. An Oxford Instruments ESR 900 helium flow cryostat in combination with an ITC 503S temperature controller was used for measurements in the 4.5–300 K range. A liquid nitrogen finger Dewar was fitted to the cavity for 77 K measurements. Instrument conditions were: microwave frequency of 9.386 GHz; field modulation frequency of 100 kHz; and modulation amplitude of 0.6 mT. Sample specific settings are given in the legends to the figures.

Quantitation of the spin concentration of EPR-active $S = 1/2$ species within a sample was determined by comparison of the double integral of the EPR spectrum with that of a 10 mM copper perchlorate standard (10 mM $CuSO_4$; 2 M $NaClO_4$; 10 mM HCl). The spin concentration is used in some of the figures since it is correlated to the total amount of protein that contains a [4Fe-4S] cluster, where the maximal amount is set at one. When multiple paramagnetic species were present in the samples, a spectrum that had only one of the species was subtracted from the overlapping spectrum to get the second spectrum and vice versa. If this was not possible, the individual signals were simulated. The software packages developed by either S. P. J. Albracht or W. Hagen were used for spectral simulation and double integration of the signals.[51,52]

The Curie plots were made by taking the signal intensity of the samples (I_0, either the height of a single peak or the double integral value) and calculate the normalized value for the intensity (I_n) by correcting for differences in power (in dB), temperature (T), and gain using the formula:

$$I_n = \frac{(I_0 \cdot T \cdot 10^{\mathrm{dB}/20})}{\mathrm{gain}} \quad (1)$$

Finally, the quantitative simulations of the $S = 1/2$ and $3/2$ EPR signals observed for the reduced, $[4Fe\text{-}4S]^+$ clusters were obtained using the SpinCount spectral analysis software developed by M. Hendrich at Carnegie Mellon University (http://www.chem.cmu.edu/groups/hendrich/facilities/index.html).

ENDOR Sample Preparation. To determine the electronic properties of the reaction intermediate species **Int**, ^{57}Fe-enriched wild type IspH from *P. falciparum* was analyzed with ENDOR. IspH with a protein concentration of 8.2 mM and 20.8% cluster content was incubated with excess (50 mM) sodium dithionite to produce the **Red** sample. In a separate experiment, the excess dithionite was removed using a PD-10 column to obtain the **Int** form of the enzyme. The intermediate signal was induced by incubating the one-electron-reduced IspH with 33 mM HMBPP for 25 s in an ENDOR tube. The incubation was stopped by freezing the sample in liquid nitrogen. The spin concentration of the signal was 0.2 mM. The **Red+P** sample was prepared by adding 30 mM IPP to the **Red** sample. The samples were stored in liquid nitrogen and transported in a liquid nitrogen dry-shipper (Taylor-Wharton, Minnetonka, MN).

EPR and ENDOR samples with IspH from *E. coli* prepared in parallel to the Mössbauer samples are described below in the Mössbauer Studies section.

Q-Band EPR/ENDOR Data Collection and Analysis. 35 GHz ("Q"-band) CW and pulsed (electron-spin–echo-detected) EPR and ^{57}Fe ENDOR spectra were recorded at 2 K in a liquid-helium bath cryostat on instruments described earlier.[53,54] The ^{57}Fe ENDOR spectra employed RF bandwidth broadening as described earlier.[55] Pulsed ^{57}Fe ENDOR spectra employed the standard Davies sequence.[56] The ENDOR spectrum of a single orientation of an $I = 1/2$ nucleus with hyperfine coupling dominant over Larmor frequency, such as ^{57}Fe, is a doublet centered at $|A(^{57}\mathrm{Fe})/2|$ and split by $2\nu(^{57}\mathrm{Fe})$ (~4 MHz here).[57,58] Full hyperfine tensors were obtained by collection and analysis of 2D field-frequency patterns of ENDOR spectra collected across an EPR spectrum as described elsewhere.[57,58]

Signs of the hyperfine couplings measured from ENDOR spectra (more specifically, the sign of $g_{\mathrm{Nuc}}A_{\mathrm{Nuc}}$) have been obtained by application of the Pulse-Endor-SaTuration-REcovery (PESTRE) protocol,[59] a pulse sequence comprised of multiple Davies ENDOR sequences, carried out in three distinct experimental phases: (I) an EPR saturation phase (RF off) of n_I Davies sequences whose spin–echo intensities quickly converge to the steady-state "baseline" (BSL); (II) an ENDOR perturbation phase of n_{II} sequences, in which each sequence contains a fixed RF value set at one or the other of the $\nu_\pm$ branches of the ENDOR spectrum; (III) and an EPR recovery phase (RF off) of n_{III} sequences during which the spin echo corresponds to the spin–echo "dynamic reference level" (DRL) associated with ENDOR-induced spin polarization created in the second phase, with the DRL relaxing to the BSL during this phase.

In the slow-relaxation regime, the sign of A_{Nuc} is unambiguously given by the sign of the difference between the DRL and BSL echo intensities in phase III of a PESTRE trace, as observed for *either* ENDOR branch. For ^{57}Fe, $g_N > 0$, so we describe *only* this case. When the PESTRE experiment is applied to the ν_+ branch and the DRL relaxes to the BSL from *below*, then $A > 0$. Conversely, when the DRL relaxes to the BSL from *above*, then $A < 0$. These inequalities are reversed when this protocol is applied to the ν_- branch.

Mössbauer Sample Preparation and Data Collection. To determine the oxidation state and electronic structure of the different $[4Fe\text{-}4S]^{n+}$ species, various samples of ^{57}Fe-enriched IspH from *E. coli* have been analyzed using Mössbauer spectroscopy. The **Red** sample was obtained by mixing the enzyme with excess sodium dithionite (50 mM). The concentration was 4.5 mM IspH and there is a 58% cluster content. The **Int** sample was identical with the **Red** sample but an additional 10-fold excess of substrate (HMBPP) was added followed by incubation for 30 s before flash freezing in ethanol. The signal concentration of the **Int** species was only 0.032 mM—too low for

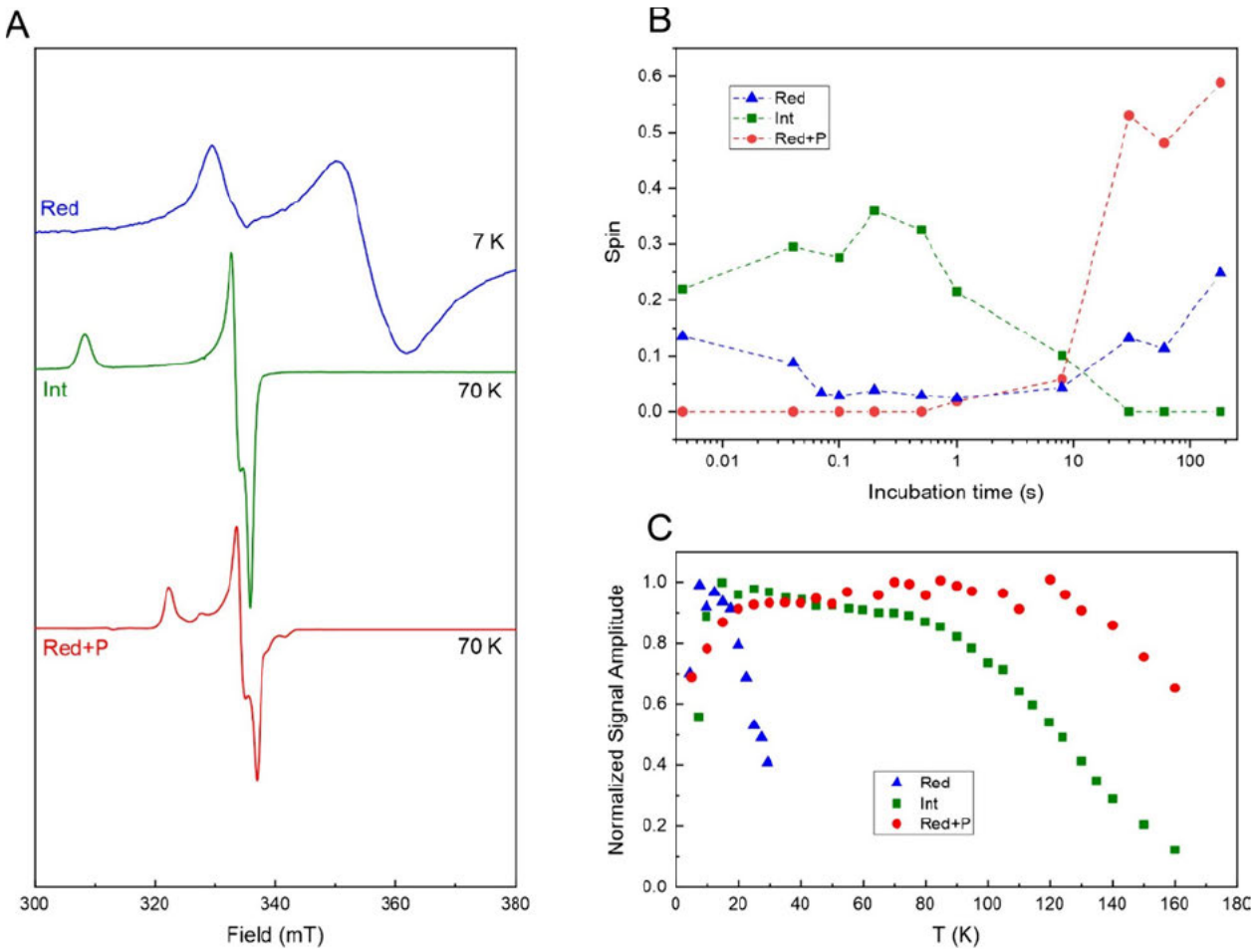

Figure 3. Overview of the intensity of paramagnetic species in rapid-freeze-quench (RFQ) studies of WT IspH. Multiple (10×) turnover experiments with 165 μM IspH (corrected for cluster content), 1.65 mM HMBPP, and 33 mM dithionite. (A) EPR signals for the observed species. The blue trace is the $[4Fe\text{-}4S]^{+}$ cluster (**Red**). The green trace is the $[4Fe\text{-}4S]^{3+}$-intermediate species (**Int**). The red trace is the $[4Fe\text{-}4S]^{+}$-IPP/DMAPP species (**Red+P**). (B) Plot of signal intensity (normalized for cluster content) vs time for the signals displayed in panel A. (C) Curie plots for the signals displayed in panel A. Enzyme from *E. coli*.

measurements. Instead, another sample was prepared by reduction with excess dithionite (50 mM), which was then removed over a PD10 column and the sample reconcentrated. A 10-fold excess of substrate (33 mM) was added followed by 30 s incubation. The concentration of the $S = 1/2$ cluster associated with the **Int** signal was determined to be 0.8 mM using spin quantitation. Samples of the EPR silent, oxidized species were prepared by mixing as-isolated IspH with either only buffer (sample **Ox**), or HMBPP (sample **Ox+S**). Both samples were 2.0 mM with a cluster content of 52%. The EPR-active species resulting from incubating reduced enzyme with product (**Red+P**) was prepared by adding excess IPP to dithionite reduced IspH. The enzyme was 1.8 mM, 52% cluster content and 0.67 mM product EPR signal was detected using spin quantitation. All samples were split and transferred to a Mössbauer cup and an EPR tube that were frozen simultaneously, in less than 30 s, in liquid nitrogen and cold ethanol, respectively. All samples were stored in liquid nitrogen and were transported in a nitrogen dry shipper.

The ^{57}Fe Nuclear Gamma Resonance (Mössbauer) spectra were recorded using a spectrometer operated in a constant acceleration mode. This instrument was equipped with a liquid-helium cooled Janis 8DT cryostat and a superconducting coil manufactured by American Magnetics. Using this setup, spectra could be recorded at temperatures ranging from 1.7 to 220 K and magnetic fields of up to 8 T. The magnetic fields were applied parallel to the direction of the 14.4 keV γ-ray beam. The light source had an activity of ~100 mCi and consisted of ^{57}Co dispersed in a rhodium metal foil. Isomer shifts are reported with respect to the center of a spectrum recorded for an α-iron metal foil. Spectra recorded at 4.2 K were obtained by submerging the absorber in liquid helium. Those recorded at higher temperatures were recorded using a Cryocon 32B temperature controller while keeping the sample in a flow of gas. Data analysis, including spectral simulations, were performed using C-based, Igor Pro codes developed in-house and the WMOSS software (See Co., formerly known as Web Research Co., Edina MN, https://www.seeco.us/).

The Mössbauer spectra were analyzed using the Hamiltonian of eq 2 which is obtained by combining the electronic spin-Hamiltonian of eq 3a with that of eq 3b which accounts for the ^{57}Fe hyperfine interactions, including the quadrupole splitting, which is the energy separation and relative order of the two Kramers doublets of the $I = 3/2$ excited nuclear state of ^{57}Fe nuclei. The ground state spins of the Fe−S clusters analyzed in this study ranged from $S = 0$ to $S = 3/2$.

$$\hat{H} = \hat{H}_e + \hat{H}_{hf} \tag{2}$$

$$\hat{H}_e = D\left[\hat{S}_z^2 - \frac{1}{3}S(S+1) + \frac{E}{D}(\hat{S}_x^2 - \hat{S}_y^2)\right] + \mu_B \vec{\hat{\mathbf{S}}}\cdot\tilde{\mathbf{g}}\cdot\vec{\mathbf{B}} \tag{3a}$$

$$\hat{H}_{hf} = \sum_{i=1}^{n}\left\{\delta_i + \frac{eQV_{zz,i}}{12}[3\hat{I}_z^2 - I_i(I_i+1) + \eta(\hat{I}_x^2 - \hat{I}_y^2)] + \vec{\hat{\mathbf{S}}}\cdot\tilde{\mathbf{A}}_i\cdot\vec{\hat{\mathbf{I}}}_i - \mu_n g_n \vec{\hat{\mathbf{I}}}_i\cdot\vec{\mathbf{B}}\right\} \tag{3b}$$

Table 1. EPR Parameters and ENDOR-Derived ^{57}Fe Hyperfine Coupling Tensors Obtained for the $S = 1/2$ Clusters of the Red, Int, and Red+P Samples

IspH state	g_x	g_y	g_z	g_{avg}	A_x [MHz]	A_y [MHz]	A_z [MHz]	A_{iso} [MHz][a]	site (type)
Red	1.899	1.899	2.036	1.945	+20	+20	+12	+17.3	$[Fe^{2+}]_2$
					−34	−34	−28	−32	$[Fe^{2.5+}]_2$
Int	2.175	2.010	1.997	2.061	+12.0	+22.0	+27.5	+20.5	Fe_4^{3+}
					+30.3	+29.5	+28.5	+29.4	Fe_3^{3+}
					−27.0	−35.0	−36.0	−32.7	$Fe_2^{2.5+}$
					−32.5	−38.0	−35.9	−35.9	$Fe_1^{2.5+}$
Red+P	2.084	2.010	1.993	2.029	+22.8	+26.8	+27.2	+25.6	Fe_4^{3+} or Fe_4^{2+}
					+17.6	+24.4	+25.2	+22.5	Fe_3^{3+} or Fe_3^{2+}
					−33.2	−37.4	−40.4	−37.0	$Fe_2^{2.5+}$
					−32.0	−35.0	−40.4	−35.8	$Fe_1^{2.5+}$

[a]Isotropic coupling constants were obtained as $A_{iso} = (A_x + A_y + A_z)/3$.

While the first term of eq 3a accounts for the zero-field splitting (ZFS) of clusters with $S > 1/2$, parametrized using the D and E/D values, the second term accounts for the electronic Zeeman interaction. Where available, the g values were set equal to those derived from the EPR studies of the equivalent samples. All symbols used in these equations have their conventional meaning. The sum of eq 3b is taken over the number of spectral components considered such that $n = 2-4$. Because the $\tilde{\mathbf{g}}$ tensors' anisotropy is small for these $S = 1/2$ clusters, the orientation of the $\tilde{\mathbf{A}}$ and electric field gradient (EFG) tensors with respect to the $\tilde{\mathbf{g}}$ tensors could not be determined. The individual components of the local EFG tensors are determined from their asymmetry parameter, $\eta = (V_{xx} - V_{yy})/V_{zz}$, and quadrupole splitting, $\Delta E_Q = (eQV_{zz}/2)\sqrt{1 + \eta^2/3}$. For all paramagnetic clusters investigated in this study we observed slow spin relaxation rates at 4.2 K ($\tau > 10^{-6}$ s). While for most samples the relaxation rate increased with increasing temperature leading to the onset of a fast relaxation regime ($\tau < 10^{-9}$ s) for other, most notably in the case of the **Int** sample, this regime is not reached even at 220 K.

In some cases, the best spectral simulations were obtained by considering a field-dependent line width. For example, certain simulations of the high-field spectra were obtained by boosting the line width by ~50%, $\Delta\Gamma \sim 0.13$ mm/s, when switching from 0 to 8 T. This field-induced increase in the apparent line width is an experimental artifact, which can be traced to the onset of an incipient thickness effect due to the strong absorption by our samples of the 14.4 keV γ rays used to detect the Mössbauer effect. Regardless of this artifact, inspection of simulations (see for example Figures S9 and S11) which were obtained considering a fixed line width, shows that using a field-dependent Γ leads to only a marginal improvement of our theoretical spectra and that the other hyperfine structure parameters are unaffected.

RESULTS

Steady-State Kinetic Analysis. The purified IspH was checked in photometric assays. The WT *E. coli* IspH showed a specific activity of 2.16 μmol·min^{-1}·mg^{-1}, a k_{cat} of 1.29 ± 0.07 s^{-1}, a K_m of 65.9 ± 10.1 μM and a k_{cat}/K_m value of 0.02 ± 0.003 μM^{-1} s^{-1}. The values were corrected for the cluster content of the enzyme, which was around 54%. For the *P. falciparum* enzyme, the specific activity is 2.91 μmol·min^{-1}·mg^{-1}, corresponding to a k_{cat} of 0.34 s^{-1}, the K_m is 19 μM and a k_{cat}/K_m value of 0.018 μM^{-1}·s^{-1}. The cluster content was 20.8%.

EPR Studies. As-isolated enzyme showed no EPR signals, indicating that all [4Fe-4S] clusters are in the diamagnetic 2+ state and no [3Fe-4S]$^+$ clusters are present. This indicates that the low cluster content is not due to cluster breakdown but is probably related to the cells having difficulties inserting the clusters resulting in the substoichiometric amounts. For discussion we call this form "**Ox**".

The three X-band EPR signals presented in Figure 3, panel A, can each be generated from stand-alone samples of the **Ox** cluster under reducing conditions, and all three are manifestly signals associated with an $S = 1/2$ cluster (EPR parameters are summarized in Table 1; the corresponding Q-band spectra are shown in Figure S3). The **Red** state, with the characteristic signal of a [4Fe-4S]$^+$ cluster, with $g_\parallel = 2.04 > g_e > g_\perp = 1.9$ ($g_{avg} = 1.94 < g_e$), can be generated by incubating the enzyme with excess dithionite.[16] The intermediate species **Int** can be generated by addition of HMBPP after first reducing the enzyme and then removing the excess dithionite by washing or a quick separation on a PD10 column.[16,30] The [4Fe-4S]$^+$ with either IPP or DMAPP bound (**Red+P**) can be generated by simply adding an excess of either of them to the reduced protein, **Red**, or by incubating reduced IspH with HMBPP for 5−10 min. At that point the substrate is converted into IPP and DMAPP. As shown in Figure S1, all these methods produced the same EPR signal, including the minor peaks. Interestingly, although both **Int** and **Red+P** states are generated by reduction, and thus likewise contain formally [4Fe-4S]$^+$ clusters, their g-pattern is more reminiscent of a [4Fe-4S]$^{3+}$ cluster, with g_1 ($g_\parallel$) = 2.175 > g_2 = 2.010, g_3 = 1.997 (~g_e; $g_{avg} = 2.061 > g_e$) for **Int** and g_1 ($g_\parallel$) = 2.084 > g_2 = 2.010, g_3 = 1.993 (~g_e; $g_{avg} = 2.029 > g_e$) for **Red+P** (see Table 1).[44]

To relate these forms to the reaction cycle, EPR-detected RFQ experiments were performed. Reaction was initiated when IspH in the presence of excess dithionite was mixed with HMBPP, with enzyme (based on cluster content) and substrate concentrations set to a ratio of 1:10. The RFQ technique allows rapid mixing and variable incubation times before quenching the reaction by freezing in cold isopentane. As reported for IspH, photometric assays provide larger k_{cat} values because of the presence of MV as opposed to assays that contain only dithionite.[30,48,60] Since dithionite is sufficient to get activity[7] and the EPR signal of MV would block parts of the IspH-based signals, MV was left out.

Measurements at 70 K revealed the formation of two EPR active species, see Figure S2, panel A. The $S = 1/2$ quasi-axial **Int** signal appears first and its intensity increases gradually up to 0.1 s, then stays detectable up to 8 s. Despite the absence of MV, we assign the **Int** species as a reaction intermediate due to the rapid development of the EPR signal in less than a second and its transient behavior. At ~ 10 s there appears a spectrum identical with that of the **Red+P** species. The late accumulation of the **Red+P** species, arising at the time when

the assay should be running out of substrate, is thus attributed to the binding of products IPP and DMAP to the rereduced enzyme.

The same samples were also examined at 7 K (Figure S2 panel B). The **Red** EPR signal, which is visible only at this temperature, is seen promptly after mixing and is relatively intense from the earliest time, 4.6 ms, to 70 ms. The intensity of this signal becomes low in the 0.1 to 10 s time range, then finally increases after 10 s. The other signals that can be detected are due to the **Int** and **Red+P** species. Their signals are detectable at this temperature but are highly saturated causing their shape to broaden and distort. An additional signal that shows overlap with the **Red+P** signal can be detected in the time range 30 s to 3 min, but only at 7 K and not at higher temperatures. The origin of this signal is not clear. Double integration of the several signals at different temperatures shows this to be a minor species.

Overall, the data clearly indicate that the first step in catalysis involves the prompt formation and subsequent disappearance of the $[4Fe\text{-}4S]^+$ cluster (**Red**) and the concomitant formation of the reaction intermediate **Int**. After depletion of the substrate the cluster gets rereduced due to the excess dithionite and the formed products can now interact with the reduced cluster resulting in detection of the **Red+P** signal (Figure 3, panel B). To highlight the uniqueness of the **Int** and **Red+P** species suggested by their *g*-values, their respective Curie plots as well as that of the **Red** $[4Fe\text{-}4S]^+$ signal are shown in Figure 3, panel C. The **Red** species can be detected without saturation or broadening only in the 10 to 20 K region as expected for this type of cluster. The **Int** signal has a much wider range for detection, 10 to 80 K, and the **Red+P** signal a yet even wider range, 20 to 120 K.

ENDOR Studies. The 35 GHz pulsed Davies ^{57}Fe ENDOR spectrum taken at a field corresponding to g_1 of the **Int** signal of IspH is shown in Figure 4; the 35 GHz CW-EPR spectrum

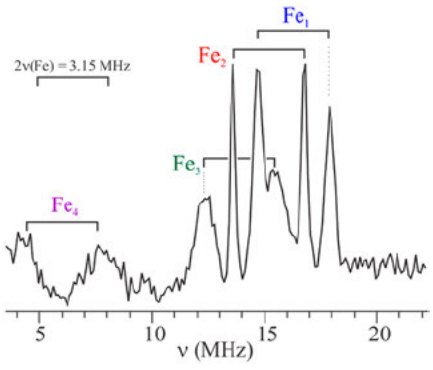

Figure 4. 35 GHz pulsed Davies ENDOR spectrum of ^{57}Fe-labeled IspH intermediate species (**Int**) recorded at g_1 and 2 K. Square brackets denote splitting of $2\nu(^{57}\text{Fe})$ between single ^{57}Fe ν_+/ν_- pairs. Conditions: Microwave frequency 34.835 GHz, magnetic field 1.1435 T (g = 2.177), microwave π pulse length 80 ns, τ = 800 ns, RF pulse length 20 μs, repetition rate 100 ms, 160 transients/point. Enzyme from *P. falciparum*.

is shown in Figure S3. The spectrum at g_1 is single-crystal-like, arising only from centers that have the external field oriented along g_1, whereas spectra at other magnetic fields arise from multiple orientations, which complicates interpretation of such spectra.[61,62] Because of the small nuclear Larmor frequency for ^{57}Fe even at Q-band, an ENDOR signal for a single molecular orientation and for a single ^{57}Fe nucleus is expected to consist of doublets centered at $A/2$, where A is the hyperfine coupling for that orientation, and split by 2ν (at g_1, 2ν = 3.15 MHz). Eight resolved peaks are observed, none of which are observed in a spectrum with an unlabeled sample, indicating that they all arise from ^{57}Fe, and it is straightforward to assign the peaks into four doublets, corresponding to the four iron ions of the cluster. These are labeled Fe_{1-4} in Figure 4, with the largest (magnitude) hyperfine coupling assigned to Fe_1 and the smallest to Fe_4. The observed g_1 hyperfine coupling values, which range from A_1 = −35.9 MHz to A_4 = 27.5 MHz, are collected in Table 1; the determination of the signs through use of the PESTRE technique[59] (see Materials and Methods) is discussed below. The full hyperfine tensors for the four ^{57}Fe sites are obtained through simulation of the spectra in a complete 2D field-frequency pattern comprised of ^{57}Fe spectra collected at fields across the entire EPR envelope of the **Int** species, Figure 5.[61,62] As shown in Figure 5, the exceptional level of resolution that remains throughout the pattern allows an accurate simulation of observed spectra in the 2D pattern through 1:1:1:1 summation of simulations that use the four high-precision hyperfine tensors listed in Table 1. We note that

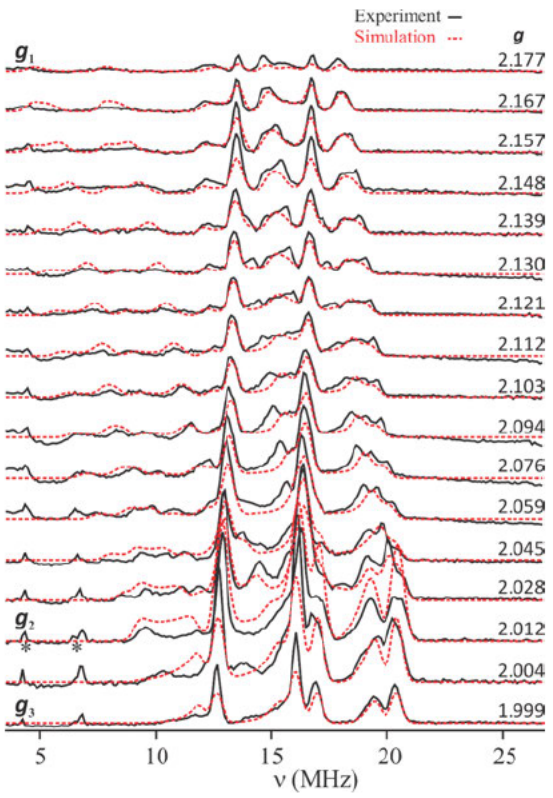

Figure 5. 35 GHz pulsed Davies ENDOR spectra of ^{57}Fe-labeled IspH intermediate species (**Int**) at 2 K, collected at the indicated g values (black), and simulations (red, dashed). EPR conditions: microwave frequency 34.834−34.884 GHz, microwave π pulse length 80 ns, τ = 800 ns, RF pulse length 20 μs, repetition rate 100 ms, 80−200 transients/point. The simulations are a 1:1:1:1 summation of four simulated spectra for the individual Fe atoms. Hyperfine couplings as in Table 1, with g = [2.174, 2.013, 1.999], EPR line width 200 MHz, ENDOR line width 0.5 MHz, and Euler angles relating g and A: γ = 90°, β = 10°, α = 5°, for Fe_1 ($A_{1/2}$ also swapped relative to Table 1), $\gamma = \beta = \alpha$ = 0° for Fe_2, γ = 15°, β = 15° for Fe_3, γ = 10° for Fe_4. The features close to 4 and 7 MHz each marked by an asterisk arise from RF harmonics output by the RF amplifier. Enzyme from *P. falciparum*.

the low frequency of the Fe_4 signal, and its high anisotropy causes it to appear with low signal/noise, but even this site could nonetheless be well fitted.

For each of the four ^{57}Fe, the simulations show that all three principal values of their hyperfine tensors have the same signs, which implies that the tensors are dominated by the isotropic hyperfine coupling, as is typical for Fe ions of Fe−S clusters. The PESTRE experiment[59] was employed to determine the absolute signs of these four hyperfine tensors, and thus of their isotropic couplings (see Materials and Methods). The multisequence PESTRE traces collected from seven of the expected eight ^{57}Fe ENDOR peaks (i.e., for both ν_+ and ν_- partners for all but Fe_4, for which only ν_- was feasible) are presented in Figure 6. The PESTRE traces indicate that the Fe

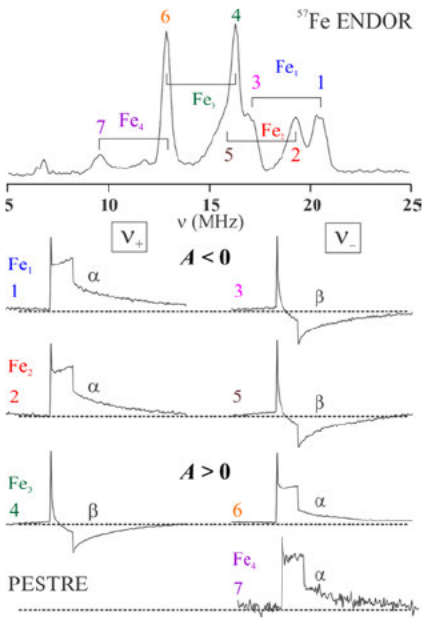

Figure 6. Determination of hyperfine signs for all four ^{57}Fe sites of labeled IspH intermediate species (**Int**) using PESTRE protocol. The determination was done at g_2 for ease of data collection; the field dependence is such that the ν_+/ν_- peaks are still well enough resolved to make sign determinations for all four iron ions. Top: 35 GHz pulsed Davies ENDOR spectrum at g_2. Bottom: PESTRE spectra recorded at each of the seven indicated positions in the ENDOR spectrum, corresponding to all four of the ν_- peaks (left; 1−3, 5), and three of the four ν_+ peaks (right; 4−7). The PESTRE response for ν_+ for Fe_4 is not measurable due to overlap with the much more intense Fe_3 peak. The PESTRE responses demonstrate that Fe_1 and Fe_2 have $A < 0$ while Fe_3 and Fe_4 have $A > 0$. Enzyme from *P. falciparum*.

sites with the larger magnitude hyperfine couplings (Fe_1, Fe_2) have negative A values, while those with the smaller couplings (Fe_3, Fe_4) have positive A values.

The analogous pulsed Davies 2D ENDOR patterns recorded for **Red+P** are presented in Figure S4 and some of those obtained for reduced IspH (**Red**) are presented in Figure S5. The hyperfine coupling constants derived from the analysis of these data are also listed in Table 1.

Mössbauer Studies. To assess the ground state spin and electronic structures of the cluster, ^{57}Fe-enriched IspH samples were prepared under different conditions and were examined with Mössbauer spectroscopy.

*As Isolated IspH (**Ox**) and HMBPP-Incubated IspH (**Ox+S**).* These states have been measured before by other groups.[60,63,64] Therefore, our detailed analysis of the spectra obtained for these species is presented in the Supporting Information. It is important to emphasize that our results reproduce the published data, providing confidence in the methods applied which reveal anomalous behavior of the clusters in their different reduced forms. The spectra obtained at different fields and temperatures for the as-isolated diamagnetic $[4Fe\text{-}4S]^{2+}$ (**Ox**) state of IspH from *E. coli*, originate from the overlap of three spectral components with a 2:1:1 relative area (Figures S6−S9). Moreover, the field dependent Mössbauer spectra demonstrate that these clusters have $S = 0$ ground state. The dominant spectral component appears as a quadrupole doublet in the zero field spectra and originates from a valence delocalized $S = 9/2$ $(Fe^{2.5+})_2$ subcluster for which the two local iron spins are ferromagnetically coupled. The second doublet exhibits parameters characteristic of tetrahedral, iron−sulfur, high spin Fe^{3+} sites, and the third originates from an atypical iron(II) site with parameters usually observed for high-spin Fe^{2+} ions supported by N/O ligands. This observation is consistent with the NRVS measurements, which revealed an atypical octahedral iron site that incorporates three water molecules and three bridging sulfide anions.[32] Incubation of the as-isolated IspH diamagnetic $[4Fe\text{-}4S]^{2+}$ cluster with HMBPP (**Ox+S**) induces a large change in the spectral component associated with the atypical iron(II) site and smaller changes for the components associated with the other three iron sites (Figures S6, S10−S12 and Table S2). These alterations are induced by the coordination of the HMBPP through the hydroxyl oxygen as shown in the crystal structure of this form of the enzyme.[19]

*Reduced IspH (**Red**).* The zero-field Mössbauer spectra recorded at 4.2 K for the dithionite reduced IspH, $[4Fe\text{-}4S]^{+}$ cluster exhibit a broad magnetic hyperfine splitting pattern which extends from −2 to +3 mm/s, see Figure S13. A spontaneous magnetic hyperfine splitting is typically observed for Kramers systems in a slow relaxation regime and is consistent with the EPR detection of $S = 1/2$ and 3/2 spin systems. Above 15 K, this pattern collapses into a broad quadrupole doublet, which at 50 K has an apparent isomer shift $\delta \approx 0.55$ mm/s and a quadrupole splitting $\Delta E_Q \approx 1.15$ mm/s, see Figures 7, S13 and Table S4. The disappearance of the magnetic hyperfine splitting may be traced to a change in the relaxation rate of the electronic spin from a slow relaxation regime at 4.2 K, $1/\tau > 10^{-6}$ s^{-1}, to a fast relaxation regime at $T \geq 30$ K, $1/\tau < 10^{-8}$ s^{-1}. The observed δ is fairly typical of $[4Fe\text{-}4S]^{+}$ clusters which have an average isomer shift $\delta_{ave} \approx 0.55$−0.60 mm/s, see Table S3.[65−68] While the mixed-valence and diferrous pairs of some reduced clusters exhibit distinct quadrupole doublets, in some cases, such as for IspH, only a single doublet is observed. However, the doublets of reduced IspH have broad resonances, which are best described using a Gaussian line shape and dissimilar line widths, $\Gamma_R/\Gamma_L \sim 0.5/0.6$ mm/s. Although these resonances become somewhat sharper at higher temperatures, their widths are still much larger than those anticipated for a homogeneous species for which we expect a Lorentzian line shape and $\Gamma \sim 0.3$ mm/s. Consequently, the experimental $T \geq 50$ K, 0 T spectra may be decomposed in two quadrupole doublets with equal spectral areas using either a nested or an intercalated pattern, see Figure S14 and Table S5. While in the first case we obtain°a°pair°of isomer shift values, $\delta_1 = 0.58$ mm/s and $\delta_2 = 0.55$ mm/s, which are similar to those of the reduced $S = 1/2$ $[4Fe\text{-}4S]^{+}$ cluster of the Fe protein from *Azotobacter*

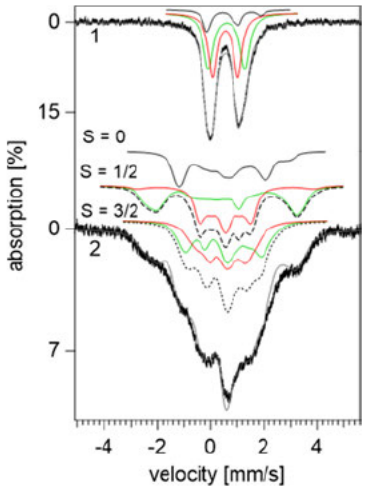

Figure 7. Mössbauer spectra of the dithionite reduced, $[4Fe\text{-}4S]^{+}$ cluster of IspH (**Red**) recorded at 50 K, 0 T (1) and 4.2 K, 8 T (2). While the experimental data are represented using vertical error bars the theoretical spectra are shown as solid gray lines. These simulations were obtained using the parameters listed in Table 2 and account for the contributions of 7 different sites distributed among clusters with $S = 0$ which have 3 sites shown in black (19%), $S = 1/2$ incorporating 2 sites shown using dashed lines (37%), and $S = 3/2$ with 2 sites represented using dotted lines (44%). The $S = 0$ spectral component originates from the $[4Fe\text{-}4S]^{2+}$ clusters of the as-isolated IspH. The contribution of the $(Fe^{2.5+})_2$ sites is shown in red and those of the $(Fe^{2+})_2$ in green, see text. Enzyme from *E. coli*.

vinelandii,[69] in the second case we obtain values, $\delta_1 = 0.68$ mm/s and $\delta_2 = 0.45$ mm/s, which are reminiscent of those derived for the $S = 3/2$ F_x cluster of the *Helicobacter* Reaction Center of *Helicobacteria*.[70]

Our analysis of the field dependent spectra, detailed in the SI, suggests that a nested arrangement of quadrupole doublets describes best the zero-field spectra of reduced IspH, see Figure 7. Thus, the field dependent Mössbauer spectra obtained for reduced IspH (**Red**), shown in Figure S15, were rationalized by considering the hyperfine coupling constants derived for the $S = 1/2$ $[4Fe\text{-}4S]^{+}$ clusters of **Red** determined from the 35 GHz ^{57}Fe ENDOR spectra, see Figure S5 and Table 1, as well as by analyzing the X-band EPR signals observed at $g \sim 5.4$ and 1.2 for **Red**, see Figures S16 and S18. The later resonances originate from $[4Fe\text{-}4S]^{+}$ clusters which have an $S = 3/2$ ground state that exhibits a relatively large ZFS such that $D \sim -7$ cm^{-1} and $E/D \sim 0.19$, see Figure S17. The presence of a mixture of $[4Fe\text{-}4S]^{+}$ clusters with different $S = 1/2$ and $S = 3/2$ ground spin states is not unique to **Red** and has been observed for other reduced, $[4Fe\text{-}4S]^{+}$ clusters including for the Fe protein from *Azotobacter vinelandii*, see Table S3.[71−73] Our simulations presented in Figures 7 and S15 suggest that while the $S = 1/2$ clusters account for ~37%, the $S = 3/2$ clusters account for 44% of the iron present in our **Red** sample, see Table 2. The remaining ~19% of the iron appears as $S = 0$, $[4Fe\text{-}4S]^{2+}$ clusters (**Ox**) which are not observed in the EPR and ENDOR spectra. To reduce the number of variables, in keeping with previous investigations, when analyzing the contribution of the $S = 3/2$ $[4Fe\text{-}4S]^{+}$ clusters, we have assumed isotropic A tensors.[69,70] Furthermore, we have employed the δ and ΔE_Q values derived for the $S = 1/2$ clusters. Using these assumptions, we have been able to reproduce the experimental spectra reasonably well by setting $A_{iso} = -11.9$ MHz for the diferrous pair and $A_{iso} = -8.9$ MHz for the mixed valence subcluster of the $S = 3/2$ species, see Table 2. Because the spectral signature of these clusters is not well resolved, in this analysis we aimed to employ a minimal number of spectral parameters. The parameter set used to

Table 2. Hyperfine Coupling Parameters Derived from the Analysis of the Mössbauer Spectra Collected for IspH[a]

sample	S	site	δ [mm/s]	ΔE_Q [mm/s]	η	A_x [MHz]	A_y [MHz]	A_z [MHz]	rel. area
Ox: $[4Fe\text{-}4S]^{2+}$	0	Fe^{2+}	0.91(1)	1.93(7)	0.5(2)		n.a.		1
		Fe^{3+}	0.32(3)	1.05(3)	0.3(2)				1
		$[Fe^{2.5+}]_2$	0.46(1)	1.18(5)	0.86(3)				2
Ox+S: substrate-bound $[4Fe\text{-}4S]^{2+}$	0	Fe^{2+}	0.64(1)	1.21(3)	0.9(1)		n.a.		1
		Fe^{3+}	0.40(2)	−0.88(3)	0.7(2)				1
		$[Fe^{2.5+}]_2$	0.43(1)	1.35(2)	0.8(3)				2
Red: reduced[b,c] $[4Fe\text{-}4S]^{1+}$	1/2 (37%)	$[Fe^{2+}]_2$	0.60	1.37	0.2[e]	+13.4	+13.4	+27.4	1
		$[Fe^{2.5+}]_2$	0.55	0.94	1.0[f]	*−34*	*−28*	*−34*	1
	3/2[d] (44%)	$[Fe^{2+}]_2$	0.60	1.37	0.0[g]	−11.9	−11.9	−11.9	1
		$[Fe^{2.5+}]_2$	0.55	0.94	0.1[h]	−8.9	−8.9	−8.9	1
Int $[4Fe\text{-}4S]^{3+}$	1/2 (50%)	$[Fe^{2.5+}]_2$	0.46(4)	1.3(1)	0.4(3)[i]	−27.0	−35.9	−35.9	1
		$[Fe^{3+}]_2$	0.37(3)	0.8(1)	1.0(4)[j]	+30.2	+28.0	+28.0	1
Red+P $[4Fe\text{-}4S]^{1+}$	1/2	Fe^{2+}	0.69(4)	2.00(5)	0.8(4)[k]	*17.6*	*24.4*	*25.2*	1
		Fe^{3+} (Fe^{2+})	0.30(5)	2.05(5)	0.6(4)[k]	*22.8*	*26.8*	*27.2*	1
		$[Fe^{2.5+}]_2$	0.48(2)	1.18(7)	0.5(5)[k]	*−32.6*[l]	*−36.2*[l]	*−40.4*[l]	2

[a]The A values shown in italics were derived from ENDOR. The numbers in parentheses denote the estimated error of the last digit. The simulations of the $S = 1/2$ species used the g tensors listed in Table 1. [b]Above 15 K the zero-field spectra consist of a single quadrupole doublet with broad resonances, see text. [c]Approximately 19% of the iron present in the sample originates from diamagnetic $[4Fe\text{-}4S]^{2+}$ clusters that were simulated using the parameters derived for the as-isolated IspH, substrate-free $[4Fe\text{-}4S]^{2+}$ clusters. [d]This spectral component is associated with the 5.4 and 1.2 effective g values and was simulated using $D = -7$ cm^{-1} and $E/D = 0.19$, see text. [e]The EFG tensor was rotated away from the A tensor using $\alpha = 14°$, $\beta = 73°$ and $\gamma = 0°$. [f]The EFG tensor was rotated away from the A tensor using $\alpha = 51°$, $\beta = 46°$ and $\gamma = 0°$. [g]The EFG tensor was rotated away from the A tensor using $\alpha = 90°$, $\beta = 70°$ and $\gamma = 0°$. [h]The EFG tensor was rotated away from the A tensor using $\alpha = 21°$, $\beta = 60°$ and $\gamma = 0°$. [i]The EFG tensor was rotated away from the A tensor using $\alpha = 0°$, $\beta = 0°$ and $\gamma = 60°$. [j]The EFG tensor was rotated away from the A tensor using $\alpha = 0°$, $\beta = 60°$ and $\gamma = 90°$. [k]The EFG tensor was rotated away from the A tensor using $\alpha = 0°$, $\beta = 90°$ and $\gamma = 0°$. [l]These values were obtained by taking the average of the corresponding (negative) values derived from ENDOR.

describe these spectra is not unique and inspection of Table S3 shows that this set of **Red** parameters is similar to those derived for other $[4Fe\text{-}4S]^{+}$, $S = 1/2$ and $S = 3/2$ clusters.

*HMBPP-Incubated Reduced IspH (**Int**).* To probe the electronic structure of the paramagnetic HMBPP-induced intermediate **Int**, one-electron-reduced **Red** state of ^{57}Fe labeled wild type enzyme (*E. coli*) was incubated with HMBPP for 30 s and the reaction was stopped by freezing the sample in liquid nitrogen.

The sample incorporated two magnetically distinct [4Fe-4S] cluster types, one paramagnetic and another with an $S = 0$ ground state. The latter species accounted for about half of the iron content. This led to Mössbauer spectra that had a lower resolution than those of other samples investigated in this study. In addition, this sample also contained an unidentified iron species with an associated subspectrum, which accounted for ~5% of the total spectral area. The most prominent feature of this spectral component is an essentially featureless°absorption observed in the high energy range, 2.8−4.0°mm/s, of the high-temperature zero-field and of the 1−2 T spectra recorded at 4.2 K. Inspection of Figures 8 and S19 shows that the

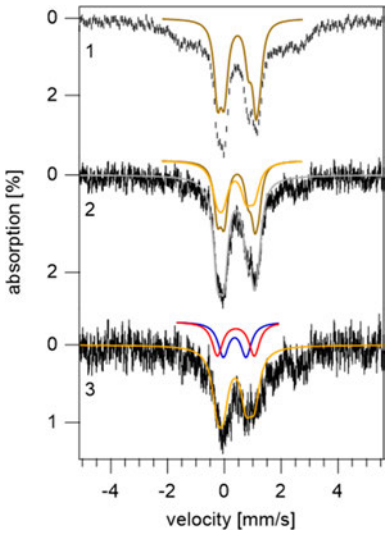

Figure 8. Zero-field temperature-dependent spectra recorded at 4.2 (1) and 150 K (2) for the Mössbauer sample associated with the intermediate (**Int**) signal. The solid brown traces drawn above (1) and (2) are theoretical spectra of the $S = 0$ clusters. While the solid orange curves drawn above (2) and over (3) account for the contribution of the $S = 1/2$ clusters, the gray trace overlaid on the experimental spectrum (2) accounts for contribution of both cluster types. The 150 K, 0 T experimental spectrum of the **Int** species (3) was obtained by subtracting the contribution of the $S = 0$ clusters. Shown in red is the contribution of the $(Fe^{2.5+})_2$ mixed valence sites and in blue, drawn above (3), that of the $(Fe^{3+})_2$ sites. The sum of these subspectra is shown in orange above (2) and over (3). Enzyme from *E. coli*.

contribution of the $S = 0$ clusters is well reproduced using the parameters determined for the as-isolated IspH incubated with HMBPP (**Ox+S**), see Table 2. Raising the temperature leads to the collapse of the magnetic hyperfine splitting pattern of the paramagnetic species into a broad quadrupole doublet. The broadening is due to the persistence of unresolved magnetic hyperfine interactions and is traced to the onset of an intermediate relaxation regime of the electronic spin. Because the paramagnetic species failed to reach a fast relaxation regime, even at 180 K, their zero-field Mössbauer parameters, δ and ΔE_Q, have been determined from the analysis of the low-temperature, field-dependent data. However, our simulations of the 150 K, 0 T spectrum such as those presented in Figure 8, obtained by capping line widths at 0.45 mm/s, corroborate the values we derived from the low temperature spectra.

The observation of a component with an unquenched magnetic hyperfine splitting at low temperature in zero field is indicative for the presence of a Kramers system with a slow relaxation regime. Inspection of Figures 9 and S19−S20 shows

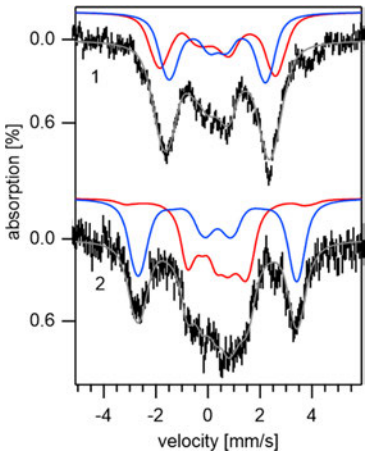

Figure 9. Field-dependent Mössbauer spectra of the $[4Fe\text{-}4S]^{3+}$ intermediate (**Int**) generated by incubating the one-electron reduced ^{57}Fe enriched *E. coli* IspH with HMBPP recorded at (1) 4.2 K, 1 T and (2) 4.2 K, 8T. The hatched and solid gray lines are the experimental data and simulation, respectively. The experimental spectra were obtained by removing the contribution of the $S = 0$ $[4Fe\text{-}4S]^{2+}$ clusters, see text. Shown in red is the spectral component associated with $(Fe^{2.5+})_2$ and in blue that of the $(Fe^{3+})_2$ subclusters. Enzyme from *E. coli*.

that, indeed, the spectroscopic behavior of the paramagnetic [4Fe-4S] clusters is well rationalized by an $S = 1/2$ spin state such as that revealed by the EPR and ENDOR studies. Moreover, these clusters exhibit two spectral components with essentially equal areas, one characterized by positive and the other by negative hyperfine coupling constants. Because of its inward moving resonances, the latter component is largely obscured by the contribution of the $S = 0$ clusters in the high-field spectra. Furthermore, at low fields the two spectral components overlap such that their outer resonances are differentiated only for $B \geq 4$ T. Due to these factors there are a limited number of spectral features that can be unambiguously assigned to the component characterized by negative A values. However, regardless of its oxidation state, an $S = 1/2$ [4Fe-4S] cluster such as that observed here is expected to incorporate at least one $S = 9/2$ mixed-valence $[Fe^{2.5+}]_2$ pair. As a consequence of its large value, the spin of this mixed valence pair is dominant and its associated spectral component is described by negative hyperfine coupling constants. Therefore, we favored solutions that yielded, for this component, zero-field Mössbauer parameters similar to those observed for the delocalized $[Fe^{2.5+}]_2$ mixed-valent pairs of $[4Fe\text{-}4S]^{2+}$ IspH clusters, see Table 2. Interestingly, the isomer shift derived for the component characterized by positive A values is smaller than that of $[Fe^{2.5+}]_2$ sites which suggests that it originates from $[Fe^{3+}]_2$ sites and that we observe a $[4Fe\text{-}4S]^{3+}$ cluster

such as those of HiPIP enzymes (Table S1).[74,75] Unlike for ENDOR, the analysis of the Mössbauer data did not allow us to differentiate the individual spectra of all four iron sites. Instead, we could distinguish only two spectral components each accounting for two iron sites, *vide supra*. However, our simulations of the field dependent Mössbauer spectra provided solutions, which, irrespective of the model used, were consistent with those derived from ENDOR, see Table S6 and Figure S20. For example, the theoretical spectra of Figure 9 and S19 and the corresponding parameters listed in Table 2 were obtained using a least-squares fitting procedure for which the individual **A** tensor components were limited to the range bracketed by the corresponding ENDOR-derived A values. While in this case we obtained axial **A** tensors with A_{iso} values that differed by 4−15% from the analogous ENDOR quantities, listed in Table 1, the observed differences are not due to intrinsic discrepancies between the two experimental methods but rather are traced to the lower resolution of the **A** tensors as obtained from Mössbauer. Regardless of these difficulties, an important result of our analysis is that the average isomer shift measured for the [4Fe-4S] clusters of **Int**, δ_{ave} = 0.40(2) mm/s, is considerably lower than those observed for the $[4Fe\text{-}4S]^{2+}$ clusters of IspH, δ_{ave} = 0.47−0.54 mm/s. This observation, like the EPR spectrum itself (see above), is more characteristic of a $[4Fe\text{-}4S]^{3+}$ cluster. However, the δ_{ave} of the **Int** signal is somewhat larger than the typical average isomer shift observed at 4.2 K for $[4Fe\text{-}4S]^{3+}$ clusters of HiPIP proteins, δ_{ave} = 0.31(3) mm/s. Undoubtedly, this difference may be traced to the influences of the bonding in the heteroleptic coordination of the atypical iron site of IspH, as pictured in Figures 1−2.

*Product Incubated Reduced IspH (**Red+P**).* The spectra recorded for the **Red+P** sample exhibit magnetic hyperfine splitting patterns irrespective of the temperature and the field at which they were obtained; see Figures 10 and S21−S23. Such zero-field spectra are typically observed at low temperature for Kramers systems in a slow spin relaxation regime, which exhibit an electronic spin flip rate lower than $1/\tau = 10^6$ s^{-1}. This behavior is consistent with the S = 1/2 spin state derived from the EPR and ENDOR measurements. Increasing the temperature boosts the relaxation rate and typically leads to the onset of a fast relaxation regime ($1/\tau > 10^8$ s^{-1}) such that in zero-field the magnetic hyperfine interactions are averaged out and only quadrupole doublets are observed. In contrast, in this case, a slow relaxation regime is still in effect even at 80 K, see Figure 10. Raising the temperature further, up to 220 K, which is the highest temperature at which the EPR signal of **Red+P** persists, leads to spectra with unresolved features and broad tails which are characteristic of an intermediate relaxation regime, see Figures S21−S22. Because of this behavior the δ and ΔE_Q values could be determined only from the spectra recorded at low temperatures.

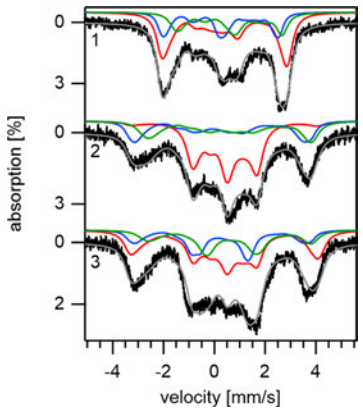

Figure 10. Selected field- and temperature-dependent Mössbauer spectra recorded for the product incubated reduced IspH sample (**Red+P**), where (1) 4.2 K, 0.1 T, (2) 4.2 K, 8 T and (3) 80 K, 8 T. The experimental data are shown using vertical error bars and the theoretical spectra are shown as solid gray traces. The individual spectral components were obtained using the parameters listed in Table 1 and were used to generate the theoretical spectra overlaid over the experimental data. Shown in red is the contribution of the $(Fe^{2.5+})_2$ subcluster; blue and green represent the localized Fe^{3+} and Fe^{2+} sites, respectively. Enzyme from *E. coli*.

The field-dependent spectra recorded at 4.2 K for **Red+P** are well reproduced considering an S = 1/2 ground spin state, see Figures 10 and S23. Moreover, fields larger than 2 T induce the splitting of the low-field spectra in two essentially equivalent spectral components, but which have opposite sign of hyperfine couplings. The isotropic hyperfine coupling constants, $A_{positive}$ = 26(3) MHz and $A_{negative}$ = −36(1) MHz, derived from spectral simulations which considered only two components compare quite well with the analogous average values derived from the ENDOR spectra, 24.0 and −36.4 MHz respectively, see Tables 1 and S7. The hyperfine coupling constants determined at 80 K appear to be ∼5% smaller than those observed at 4.2 K, which suggests that perhaps one, or more low-lying excited spin states might be thermally accessible. A surprising feature of these simulations is that they provide similar isomer shift values for the individual spectral components and that these values are comparable to those of delocalized mixed-valence sites such as those observed for the $[Fe^{2.5+}]_2$ subclusters of the $[4Fe\text{-}4S]^{2+}$ S = 0 clusters described above. The simulated spectra presented in Figures 10 and S23 were obtained using the hyperfine coupling constants derived from ENDOR. To validate these simulations, we have used a stepwise strategy to analyze the experimental data we collected for this sample. Some of the alternative models considered are summarized in Table S7 and the corresponding simulations are presented in Figure S24. Due to their similitude and relatively small anisotropy, the two negative **A** tensors obtained from ENDOR were combined into a single unit by taking the average of their individual tensor components to generate a subspectrum, which accounted for half of the spectral area. This component is ascribed to a valence delocalized $[Fe^{2.5+}]_2$ subcluster with an S = 9/2 ground spin state. Inspection of the ENDOR-provided positive **A** tensors shows that while one of them is quasi-axial the other is not only rhombic but also exhibits considerable anisotropy. Since these tensors are reminiscent of those observed for high-spin ferric and ferrous sites, respectively, we focused on spectral simulations which provided a smaller isomer shift for the first site and a larger value for the latter, see Table 2. Consequently, we assigned the corresponding spectral components to quasi-localized Fe^{2+} and Fe^{3+} sites, respectively. Interestingly, these assignments lead not only to a 2:1:1 pattern of spectral area as observed for the **Ox** and **Ox+S** samples, but also to parameters similar to that of 4Fe clusters with a 2+ oxidation state.

The S = 1/2 state of **Red+P** is doubly anomalous, in that the formally $[4Fe\text{-}4S]^{+}$ cluster has an EPR signal suggestive of a $[4Fe\text{-}4S]^{3+}$ cluster (i.e., $g_\perp \gtrsim g_e$), yet has features in its

Mössbauer spectra characteristic of an $S = 0$ state. One can try to invoke a situation where the unpaired electron is transferred to and localized over the cluster-bound substrate. This would be similar to covalently linked exchange coupled chromophores reported for the coupled chromophores of $[4Fe\text{-}4S]^{2+}$-siroheme of sulfite reductase from *E. coli*, $[4Fe\text{-}4S]^{2+}$-$[Fe_2]$ of *Desufovibrio vulgaris* hydrogenase, or for the reduced CO treated Ni-activated carbon monoxide dehydrogenase (A_{red}-CO of CODH) from *Clostridium thermoaceticum*.[76,77,66,78] However, that assignment is ruled out by the characteristics of this state showing it contains a paramagnetic cluster, as opposed to the near-isotropic g-values and substantial ^1H hyperfine splittings expected for a radical. Moreover, a comparison of spectra of the **Int** and **Red+P** EPR signals signal from enzyme purified from cells grown with natural abundance Fe or enriched in ^{57}Fe show very similar ^{57}Fe broadening (Figure 11). Although the Curie behavior of these signals (Figure 3, panel C) is unlike that of regular ferredoxin type $[4Fe\text{-}4S]^{+}$ clusters, the amount of ^{57}Fe broadening places a significant amount of the electron density on the clusters which would argue against a $[4Fe\text{-}4S]^{2+}$-product$^{\bullet-}$ explanation for the **Red+P** state.

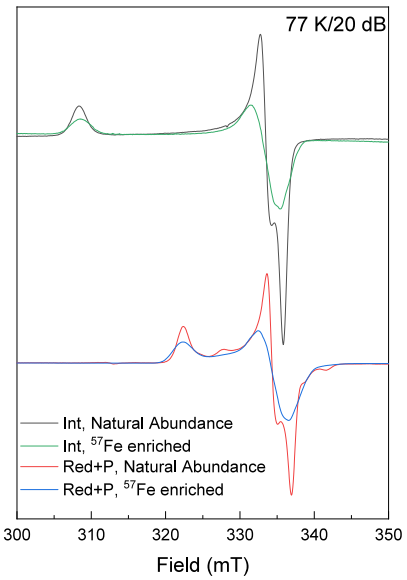

Figure 11. X-band EPR spectra of the Int and Red+P species prepared with natural abundance Fe and enriched in ^{57}Fe. The intensity of the spectra in each set has been normalized for comparison. Enzyme from *E. coli*.

DISCUSSION

EPR, ENDOR, and Mössbauer data were presented on different states in the catalytic cycle of the enzyme IspH. The two oxidized cluster ($[4Fe\text{-}4S]^{2+}$) forms, as isolated (**Ox**) and with added substrate (**Ox+S**), have been previously investigated[60,63,64] and our results agree with those studies. The $[4Fe\text{-}4S]^{2+}$ form incorporates not only sulfur-coordinated, tetrahedral iron sites including a valence-delocalized $(Fe^{2.5+})_2$ pair and a high spin Fe^{3+} site, but also a high-spin Fe^{2+} ion that is, in addition to the three bridging sulfides, ligated by nonsulfur ligands. NRVS measurements showed that this iron has an octahedral geometry with a first coordination sphere consisting of three sulfur atoms and three oxygen atoms from three water molecules.[32] Upon addition of substrate (HMBPP) only the properties of this high-spin Fe^{2+} ion are significantly modified. The changed isomer shift is characteristic of a valence-trapped Fe^{2+} site supported by a nonsulfur ligand, most likely the hydroxyl oxygen of HMBPP.[19] The field-dependent Mössbauer spectra as well as the lack of an EPR signal for both species demonstrate an $S = 0$ ground spin state for the $[4Fe\text{-}4S]^{2+}$ clusters in both **Ox** and **Ox+S**.

Addition of reducing agent, dithionite ion, to **Ox** generates the **Red** state which incorporates $[4Fe\text{-}4S]^{+}$ clusters with both $S = 1/2$ and $3/2$ ground spin states.[67] The ENDOR-derived hyperfine coupling tensors were used to rationalize the spectral components of the Mössbauer spectra associated with the $S = 1/2$ cluster. The analysis of the X-band EPR spectra suggested that the $S = 3/2$ cluster has a ZFS tensor characterized by a relatively large and negative ZFS parameter $D \approx -7\ cm^{-1}$ as well as a large rhombicity, $|E/D| \sim 0.19$. To reduce the number of parameters considered, the subspectra of the $S = 3/2$ species were reproduced using isotropic **A** tensors. Regardless, the δ and ΔE_Q values determined for these species are in line with a 1+ oxidation state for the cluster, as expected.

Our main goal here was to determine the redox state of the $[4Fe\text{-}4S]$ cluster of the **Int** species, generated by addition of the substrate HMBPP to **Red**. EPR, ENDOR, and Mössbauer data are characteristic of a $[4Fe\text{-}4S]^{3+}$ cluster with an $S = 1/2$ spin state. The Mössbauer spectra were rationalized using two components, one with $\delta = 0.46$ mm/s and $\Delta E_Q = 1.3$ mm/s, and another with $\delta = 0.37$ mm/s and $\Delta E_Q = 0.8$ mm/s. The first set of parameters are fairly typical of valence-delocalized $(Fe^{2.5+})_2$ iron−sulfur subclusters with tetrahedral metal sites. The second component is ascribed to a $(Fe^{3+})_2$ pair. The only known cluster state that can be used for comparison is the one detected in *N*-ethylmaleimide (NEM) modified Ftr.[25,28] The spectra recorded for the different NEM-modified Ftr enzymes have three components with an intensity ratio of 1:1:2 (Table S1). The dominant spectral component originates from a valence delocalized $(Fe^{2.5+})_2$ subcluster. The other two components are due to the ferric sites, consistent with the $[4Fe\text{-}4S]^{3+}$ assignment. In the $[4Fe\text{-}4S]^{3+}$ clusters in HiPIP enzymes the two ferric ions are indistinguishable, as they have nearly identical geometries (Table S1), with all Fe sites coordinated by single cysteinyl thiolate. Coordination of the additional cysteine thiol in Ftr makes the two ferric ions distinct. One ferric ion has a lower δ value, 0.29 mm/s, which is consistent with ferric sites with tetrahedral sulfur coordination.[67,79−82] The larger δ value, 0.32 mm/s, determined for the other ferric site was used as evidence of a higher coordination number. In contrast, the two ferric ions of the IspH **Int** species not belonging to the mixed-valence subcluster could be distinguished only by ENDOR but not by Mössbauer spectroscopy. This would indicate that the proposed η^3-binding of the bound intermediate does not change the electronic and magnetic properties of the unique Fe^{3+} ion which could still resemble a distorted tetrahedron.

A final species studied is that formed upon addition of product, in this case IPP, to **Red** which generates a new paramagnetic species **Red+P**. Analysis of the EPR and field dependent Mössbauer spectra indicates that this is a pure $S = 1/2$ species, in contrast to **Red** with its $S = 3/2$ component. The Mössbauer spectra of **Red+P** were thus simulated using $S = 1/2$ and the hyperfine tensors for all four cluster Fe sites derived by ENDOR. This analysis yielded δ and ΔE_Q for the dominant spectral component parameters, corresponding to two Fe sites that were typical of a sulfur-supported valence-

delocalized $(Fe^{2.5+})_2$ subcluster with tetrahedral iron, as found in $[4Fe\text{-}4S]^{2+}$, namely in an Ox type cluster. We also identified a high-spin Fe^{2+} ion supported by nonsulfur ligands with parameters similar to those determined for the atypical site of the IspH Ox and Ox+S clusters. Lastly, we obtain for the remaining iron site an isomer shift typical of high spin Fe^{3+} sites supported by sulfur ligands but with a quadrupole splitting that is unusually large for such species and is more commonly encountered for Fe^{2+} sites.

The presence of a 2+ state, which would have $S = 0$, is unambiguously contradicted by the cluster spin of $S = 1/2$, while a canonical 1+ cluster oxidation state relies *solely* on assigning a definite oxidation state to this site, making the interpretation of the Mössbauer measurements a challenge.[76,77,83] Although there is some discussion related to the 2+ interpretation in the literature,[76,77,83] the situation here is unique. The Ftr signal was initially thought to be due to a 2+ cluster and a sulfur radical. Mössbauer, however, showed it to be a 3+ cluster. Likewise, a corresponding interpretation as a $[4Fe\text{-}4S]^{2+}$-product$^{\bullet-}$ complex for the Red+P form can be discounted. The ^{57}Fe ENDOR (Figure S4) and correlated broadening of the EPR signal in the presence of ^{57}Fe (Figure 11) contradict such an assignment for Red+P. In addition, and equally, if not more telling, an organic radical would have near-isotropic g-values and give larger ^{1,2}H and ^{13}C (and if possible/appropriate ^{15}N and ^{17}O), hyperfine couplings observable in EPR and detected by ENDOR/HYSCORE in the suitable isotopologs, than observed for (*E*)-4-hydroxy-3-methylbut-2-enyl diphosphate synthase (IspG) or IspH with bound inhibitors (e.g., 0.2 MHz $\leq a_{iso}(^{13}C) \leq$ 3.6 MHz).[18] A helpful summary of a_{iso} values for selected atoms for the different proposed reaction intermediates in IspH and IspG is given in Xu et al.;[16] in only one case, for IspG with bound substrate (2-^{13}C-methylerythritol-cyclo-2,4-diphosphate, $^{13}C_2$-MEcPP) is the ^{13}C coupling appreciable, $a_{iso}(^{13}C) = 17.7$ MHz,[5] and even this value is far less than would be exhibited by a carbon-centered radical.[84,85] Very recently, Hoffman, Suess and co-workers showed that a $[4Fe\text{-}4S]^{+}$ model compound with a bound methyl group, i.e., the simplest such, directly σ-bonded organometallic species, gives $a_{iso}(^{13}C) = 5.5$ MHz.[86]

CONCLUSIONS

The present EPR/ENDOR/Mössbauer studies on multiple states of IspH showed unique properties for the Red, Int, and Red+P samples, including the display of relaxation regime that complicated the analysis. The measurements, however, conclusively show the reaction intermediate (Int) to be in a 3+ oxidation state. The signal induced by binding of the product IPP to the reduced cluster (Red+P) was more challenging. This cluster species would be assigned a 2+ state based solely on Mössbauer measurements, but its $S = 1/2$ state with large g-shifts, plus ^{57}Fe hyperfine couplings and small couplings to bound organic moieties as revealed by EPR/ENDOR, rules out such an assignment and favors a 1+ oxidation state. It is possible that the overlap between Mössbauer parameters for 1+ and 2+ species is much larger than previously expected, but it is more likely, however, that the situation for the Red+P species is unique. Here theoretical studies are called for to examine the exact distribution of electron density, as has been very recently done for bioorganometallic radical SAM enzyme intermediates.[87] DFT/SCRF computations have already been applied on the first steps in the reaction mechanism in Figure 2, indicating that reduction of the active-site clusters results in the η^2-bound state.[38] The information in the present study can thus guide future computational investigations.

Beside the insights into the unique cluster redox chemistry there are also implications for further drug development targeting IspH. It is important to realize that compounds will bind differently to the oxidized or the reduced cluster, and it is not clear what redox state should be targeted in the living cell to have the largest inhibitory effect. The buildup of the Red+P species in activity assays indicates that compounds that resemble IPP and DMAPP alkenes could be potential inhibitors, consistent with the strongest known IspH inhibitors that contain double and triple bonds,[39] although none of these are suitable drug candidates due to the highly charged phosphate groups. The most powerful inhibitors should be able to bind to both oxidized and reduced clusters and preferably trap the cluster in the 3+ state.

ASSOCIATED CONTENT

Supporting Information

The Supporting Information is available free of charge at

Additional EPR and ^{57}Fe ENDOR data; Detailed descriptions of the Mössbauer data for Ox and Ox+S states as well as additional data for the Red, Int, and Red+P states; Tables containing Mössbauer parameters of $S = 1/2$ $[4Fe\text{-}4S]^{3+}$ clusters and $S = 1/2$ $[4Fe\text{-}4S]^{1+}$ clusters found in the literature as well as the respective references (PDF)

AUTHOR INFORMATION

Corresponding Authors

Sebastian A. Stoian − *Department of Chemistry, University of Idaho, Moscow, Idaho 83844, United States;* orcid.org/0000-0003-3362-7697; Phone: (208) 885-0966; Email: sstoian@uidaho.edu

Evert C. Duin − *Department of Chemistry and Biochemistry, Auburn University, Auburn, Alabama 36849, United States;* orcid.org/0000-0002-4129-758X; Phone: (334) 844-6072; Email: duinedu@auburn.edu

Authors

Selamawit Ghebreamlak − *Department of Chemistry and Biochemistry, Auburn University, Auburn, Alabama 36849, United States;* Present Address: Alabama Department of Agriculture & Industries, State Chemical Laboratory, Auburn, Alabama 36832, United States

Nicholas S. Lees − *Department of Chemistry, Northwestern University, Evanston, Illinois 60208, United States*

Bryan Cronin − *Department of Chemistry and Biochemistry, Auburn University, Auburn, Alabama 36849, United States*

Forrest Smith − *Department of Drug Discovery & Development, Auburn University, Auburn, Alabama 36849, United States*

Matthew O. Ross − *Department of Chemistry, Northwestern University, Evanston, Illinois 60208, United States;* Present Address: Department of Chemistry, University of Chicago, Chicago, Illinois 60637, United States

Joshua Telser − *Department of Biological, Chemical and Physical Sciences, Roosevelt University, Chicago, Illinois 60605, United States;* orcid.org/0000-0003-3307-2556

Brian M. Hoffman – *Department of Chemistry, Northwestern University, Evanston, Illinois 60208, United States;* orcid.org/0000-0002-3100-0746

Complete contact information is available at:

Notes

The authors declare no competing financial interest.

■ ACKNOWLEDGMENTS

This work was supported by National Science Foundation Grants 0848196 (E.C.D.) and MCB-1908587 (B.M.H.). A portion of this work was performed at the National High Magnetic Field Laboratory, which is supported by National Science Foundation Cooperative Agreement No. DMR-2128556 and the State of Florida. In addition, thanks go out to Dr. Hassam Jomaa and Dr. Michael Groll for providing some of the expression plasmids used in this work.

■ ABBREVIATIONS

BSL, baseline signal level; dB, decibel; CODH, carbon monoxide dehydrogenase; CW, continuous wave; *D*, axial zero-field splitting parameter; DFT/SCRF, density functional theory/self-consistent reaction field; DMAPP, dimethylallyl diphosphate; DRL, dynamic reference level; *E*/*D*, rhombic zero-field splitting parameter ratio; EFG, electric field gradient; ENDOR, electron–nuclear double resonance; EPR, electron paramagnetic resonance; Fd, ferredoxin; Ftr, ferredoxin:thioredoxin reductase; HiPIP, high-potential iron–sulfur protein; HMBPP, (*E*)-4-hydroxy-3-methylbut-2-enyl diphosphate; HYSCORE, hyperfine sublevel correlation; Int, IspH showing the intermediate EPR signal; IspG, (*E*)-4-hydroxy-3-methylbut-2-enyl diphosphate synthase; IspH, (*E*)-4-hydroxy-3-methylbut-2-enyl diphosphate reductase; IPP, isopentenyl diphosphate; LB agar, Luria–Bertani agar; mT, milli Tesla; MV, methyl viologen; NEM-modified, *N*-ethylmaleimide-modified; NRVS, nuclear resonance vibrational spectroscopy; Ox, IspH in the oxidized (as purified) form; Ox+S, IspH in the oxidized (as purified) form in the presence of HMBPP; PD-10 column, desalting Sephadex G-25 column; PESTRE protocol, Pulse-Endor-SaTuration-REcovery protocol; Red, IspH in the dithionite reduced form; Red+P, IspH in the dithionite reduced form in the presence of IPP and/or DMAPP; RF, radio frequency; RFQ, rapid freeze-quench; SOC medium, super optimal medium with catabolic repressor medium; ZFS, zero-field splitting.

■ REFERENCES

(1) Beinert, H.; Kennedy, M. C.; Stout, C. D. Aconitase as iron-sulfur protein, enzyme, and iron-regulatory protein. *Chem. Rev.* 1996, *96* (7), 2335–2374.

(2) Broderick, J. B.; Duffus, B. R.; Duschene, K. S.; Shepard, E. M. Radical S-Adenosylmethionine Enzymes. *Chem. Rev.* 2014, *114* (8), 4229–4317.

(3) Adams, M. W. W.; Jenney, F. E., Jr.; Clay, M. D.; Johnson, M. K. Superoxide reductase: fact or fiction? *J. Biol. Inorg. Chem.* 2002, *7*, 647–652.

(4) Staples, C. R.; Gaymard, E.; Stritt-Etter, A.-L.; Telser, J.; Hoffman, B. M.; Schürmann, P.; Knaff, D. B.; Johnson, M. K. Role of the $[Fe_4S_4]$ cluster in mediating disulfide reduction in spinach ferredoxin:thioredoxin reductase. *Biochemistry* 1998, *37* (13), 4612–4620.

(5) Wang, W.; Wang, K.; Li, J.; Nellutla, S.; Smirnova, T. I.; Oldfield, E. An ENDOR and HYSCORE Investigation of a Reaction Intermediate in IspG (GcpE) Catalysis. *J. Am. Chem. Soc.* 2011, *133* (22), 8400–8403.

(6) Adedeji, D.; Hernandez, H.; Wiesner, J.; Köhler, U.; Jomaa, H.; Duin, E. C. Possible direct involvement of the active-site [4Fe–4S] cluster of the GcpE enzyme from *Thermus thermophilus* in the conversion of MEcPP. *FEBS J.* 2007, *581* (2), 279–283.

(7) Altincicek, B.; Duin, E. C.; Reichenberg, A.; Hedderich, R.; Kollas, A.-K.; Hintz, M.; Wagner, S.; Wiesner, J.; Beck, E.; Jomaa, H. LytB protein catalyzes the terminal step of the 2-C-methyl-D-erythritol-4-phosphate pathway of isoprenoid biosynthesis. *FEBS J.* 2002, *532* (3), 437–440.

(8) Rohmer, M. The discovery of a mevalonate-independent pathway for isoprenoid biosynthesis in bacteria, algae and higher plants. *Nat. Prod. Rep.* 1999, *16*, 565–574.

(9) Jomaa, H.; Wiesner, J.; Sanderbrand, S.; Altincicek, B.; Weidemeyer, C.; Hintz, M.; Türbachova, I.; Eberl, M.; Zeidler, J.; Lichtenthaler, H. K.; Soldati, D.; Beck, E. Inhibitors of the Nonmevalonate Pathway of Isoprenoid Biosynthesis as Antimalarial Drugs. *Science* 1999, *285* (5433), 1573–1576.

(10) Missinou, M. A.; Borrmann, S.; Schindler, A.; Issifou, S.; Adegnika, A. A.; Matsiegui, P.-B.; Binder, R.; Lell, B.; Wiesner, J.; Baranek, T.; Jomaa, H.; Kremsner, P. G. Fosmidomycin for malaria. *Lancet* 2002, *360* (9349), 1941–1942.

(11) Lell, B.; Ruangweerayut, R.; Wiesner, J.; Missinou, M. A.; Schindler, A.; Baranek, T.; Hintz, M.; Hutchinson, D.; Jomaa, H.; Kremsner, P. G. Fosmidomycin, a novel chemotherapeutic agent for malaria. *Antimicrob. Agents Ch.* 2003, *47* (2), 735–738.

(12) Borrmann, S.; Issifou, S.; Esser, G.; Adegnika, A. A.; Ramharter, M.; Matsiegui, P.-B.; Oyakhirome, S.; Mawili-Mboumba, D. P.; Missinou, M. A.; Kun, J. F. J.; Jomaa, H.; Kremsner, P. G. Fosmidomycin-clindamycin for the treatment of Plasmodium falciparum malaria. *J. Infect. Dis.* 2004, *190* (9), 1534–1540.

(13) Rohdich, F.; Bacher, A.; Eisenreich, W. Isoprenoid biosynthetic pathways as anti-infective drug targets. *Biochem. Soc. Trans.* 2005, *33*, 785–791.

(14) Eoh, H.; Brennan, P. J.; Crick, D. C. The *Mycobacterium tuberculosis* MEP (2C-methyl-D-erythritol 4-phosphate) pathway as a new drug target. *Tuberculosis* 2009, 89 (1), 1–11.

(15) Oldfield, E. Targeting Isoprenoid Biosynthesis for Drug Discovery: Bench to Bedside. *Acc. Chem. Res.* 2010, *43* (9), 1216–1226.

(16) Xu, W. Y.; Lees, N. S.; Hall, D.; Welideniya, D.; Hoffman, B. M.; Duin, E. C. A Closer Look at the Spectroscopic Properties of Possible Reaction Intermediates in Wild-Type and Mutant (*E*)-4-Hydroxy-3-methylbut-2-enyl Diphosphate Reductase. *Biochemistry* 2012, *51* (24), 4835–4849.

(17) Wang, W.; Wang, K.; Liu, Y.-L.; No, J.-H.; Li, J.; Nilges, M. J.; Oldfield, E. Bioorganometallic mechanism of action, and inhibition, of IspH. *Proc. Natl. Acad. Sci. USA* 2010, *107* (10), 4522–4527.

(18) Guerra, F.; Wang, K.; Li, J.; Wang, W.; Liu, Y.-L.; Amin, S.; Oldfield, E. Inhibition of the 4Fe-4S proteins IspG and IspH: an EPR, ENDOR and HYSCORE investigation. *Chem. Sci.* 2014, *5* (4), 1642–1649.

(19) Span, I.; Gräwert, T.; Bacher, A.; Eisenreich, W.; Groll, M. Crystal Structures of Mutant IspH Proteins Reveal a Rotation of the Substrate's Hydroxymethyl Group during Catalysis. *J. Mol. Biol.* 2012, *416* (1), 1–9.

(20) Sweeney, W. V.; Rabinowitz, J. C. Proteins Containing 4Fe-4S Clusters: An Overview. *Annu. Rev. Biochem.* 1980, *49*, 139–161.

(21) Liu, J.; Chakraborty, S.; Hosseinzadeh, P.; Yu, Y.; Tian, S. L.; Petrik, I.; Bhagi, A.; Lu, Y. Metalloproteins Containing Cytochrome, Iron-Sulfur, or Copper Redox Centers. *Chem. Rev.* 2014, *114* (8), 4366–4469.

(22) Cammack, R.; Patil, D. S.; Fernandez, V. M. Electron-spin-resonance/electron-paramagnetic-resonance spectroscopy of iron-sulphur enzymes. *Biochem. Soc. Trans.* 1985, *13*, 572–578.

(23) Antanaitis, B. C.; Moss, T. H. Magnetic studies of the four-iron high-potential, non-heme protein from *Chromatium vinosum*. *Biochim. Biophys. Acta* 1975, *405*, 262–279.

(24) Dunham, W. R.; Hagen, W. R.; Fee, J. A.; Sands, R. H.; Dunbar, J. B.; Humblet, C. An investigation of *Chromatium vinosum* high-potential iron-sulfur protein by EPR and Mössbauer spectroscopy; evidence for a freezing-induced dimerization in NaCl solutions. *Biochim. Biophys. Acta* **1991**, *1079*, 253−262.
(25) Jameson, G. N. L.; Walters, E. M.; Manieri, W.; Schürmann, P.; Johnson, M. K.; Huynh, B. H. Spectroscopic evidence for site specific chemistry at a unique iron site of the [4Fe-4S] cluster in ferredoxin:thioredoxin reductase. *J. Am. Chem. Soc.* **2003**, *125* (5), 1146−1147.
(26) Walters, E. M.; Johnson, M. K. Ferredoxin: thioredoxin reductase: disulfide reduction catalyzed via novel site-specific [4Fe-4S] cluster chemistry. *Photosynth. Res.* **2004**, *79* (3), 249−264.
(27) Johnson, M. K.; Staples, C. R.; Duin, E. C.; Lafferty, M. E.; Duderstadt, R. E. Novel roles for Fe-S clusters in stabilizing or generating radical intermediates. *Pure Appl. Chem.* **1998**, *70* (4), 939−946.
(28) Walters, E. M.; Garcia-Serres, R.; Jameson, G. N. L.; Glauser, D. A.; Bourquin, F.; Manieri, W.; Schürmann, P.; Johnson, M. K.; Huynh, B. H. Spectroscopic characterization of site-specific $[Fe_4S_4]$ cluster chemistry in ferredoxin: thioredoxin reductase: Implications for the catalytic mechanism. *J. Am. Chem. Soc.* **2005**, *127* (26), 9612−9624.
(29) Chang, W.-C.; Xiao, Y.; Liu, H.-W.; Liu, P. H. Mechanistic Studies of an IspH-Catalyzed Reaction: Implications for Substrate Binding and Protonation in the Biosynthesis of Isoprenoids. *Angew. Chem., Int. Ed.* **2011**, *50* (51), 12304−12307.
(30) Wang, W.; Wang, K.; Span, I.; Jauch, J.; Bacher, A.; Groll, M.; Oldfield, E. Are Free Radicals Involved in IspH Catalysis? An EPR and Crystallographic Investigation. *J. Am. Chem. Soc.* **2012**, *134*, 11225−11234.
(31) Frank, A.; Groll, M. The Methylerythritol Phosphate Pathway to Isoprenoids. *Chem. Rev.* **2017**, *117* (8), 5675−5703.
(32) Faus, I.; Reinhard, A.; Rackwitz, S.; Wolny, J. A.; Schlage, K.; Wille, H. C.; Chumakov, A.; Krasutsky, S.; Chaignon, P.; Poulter, C. D.; Seemann, M.; Schunemann, V. Isoprenoid Biosynthesis in Pathogenic Bacteria: Nuclear Resonance Vibrational Spectroscopy Provides Insight into the Unusual [4Fe-4S] Cluster of the E. coli LytB/IspH Protein. *Angew. Chem., Int. Ed.* **2015**, *54* (43), 12584−12587.
(33) Chaignon, P.; Petit, B. E.; Vincent, B.; Allouche, L.; Seemann, M. Methylerythritol Phosphate Pathway: Enzymatic Evidence for a Rotation in the LytB/IspH-Catalyzed Reaction. *Chem.—Eur. J.* **2020**, *26* (5), 1032−1036.
(34) Wang, W.; Li, J.; Wang, K.; Huang, C.; Zhang, Y.; Oldfield, E. Organometallic mechanism of action and inhibition of the 4Fe-4S isoprenoid biosynthesis protein GcpE (IspG). *P. Natl. Acad. Sci. USA* **2010**, *107* (25), 11189−11193.
(35) Lee, H.-I.; Igarashi, R. Y.; Laryukhin, M.; Doan, P. E.; Dos Santos, P. C.; Dean, D. R.; Seefeldt, L. C.; Hoffman, B. M. An organometallic intermediate during alkyne reduction by nitrogenase. *J. Am. Chem. Soc.* **2004**, *126* (31), 9563−9569.
(36) Brown, A. C.; Suess, D. L. M. Valence Localization in Alkyne and Alkene Adducts of Synthetic $[Fe_4S_4]^+$ Clusters. *Inorg. Chem.* **2023**, *62*, 1911−1918.
(37) Blachly, P. G.; Sandala, G. M.; Giammona, D. A.; Liu, T.; Bashford, D.; McCammon, J. A.; Noodleman, L. Use of Broken-Symmetry Density Functional Theory To Characterize the IspH Oxidized State: Implications for IspH Mechanism and Inhibition. *J. Chem. Theory. Comput.* **2014**, *10* (9), 3871−3884.
(38) Blachly, P. G.; Sandala, G. M.; Giammona, D. A.; Bashford, D.; McCammon, J. A.; Noodleman, L. Broken-Symmetry DFT Computations for the Reaction Pathway of IspH, an Iron-Sulfur Enzyme in Pathogenic Bacteria. *Inorg. Chem.* **2015**, *54* (13), 6439−6461.
(39) Wang, K.; Wang, W.; No, J.-H.; Zhang, Y.; Zhang, Y.; Oldfield, E. Inhibition of the Fe_4S_4-Cluster-Containing Protein IspH (LytB): Electron Paramagnetic Resonance, Metallacycles, and Mechanisms. *J. Am. Chem. Soc.* **2010**, *132* (19), 6719−6727.
(40) Li, J.; Wang, K.; Smirnova, T. I.; Khade, R. L.; Zhang, Y.; Oldfield, E. Isoprenoid Biosynthesis: Ferraoxetane or Allyl Anion Mechanism for IspH Catalysis? *Angew. Chem., Int. Ed.* **2013**, *52* (25), 6522−6525.
(41) Seemann, M.; Rohmer, M. Isoprenoid biosynthesis via the methylerythritol phosphate pathway: GcpE and LytB, two novel iron-sulphur proteins. *C. R. Chim.* **2007**, *10* (8), 748−755.
(42) Rius, G.; Lamotte, B. Single-Crystal ENDOR Study of a ^{57}Fe-Enriched Iron-Sulfur $[Fe_4S_4]^{3+}$ Cluster. *J. Am. Chem. Soc.* **1989**, *111* (7), 2464−2469.
(43) Moriaud, F.; Gambarelli, S.; Lamotte, B.; Mouesca, J. M. Single-crystal ^{57}Fe Q-band ENDOR study of the 4 iron-4 sulfur cluster in its reduced $[4Fe\text{-}4S]^{1+}$ state. *J. Magn. Reson.* **2001**, *153* (2), 238−245.
(44) Dilg, A. W. E.; Mincione, G.; Achterhold, K.; Iakovleva, O.; Mentler, M.; Luchinat, C.; Bertini, I.; Parak, F. G. Simultaneous interpretation of Mössbauer, EPR and ^{57}Fe ENDOR spectra of the $[Fe_4S_4]$ cluster in the high-potential iron protein I from *Ectothiorhodospira halophila*. *J. Biol. Inorg. Chem.* **1999**, *4* (6), 727−741.
(45) Kappl, R.; Ciurli, S.; Luchinat, C.; Hüttermann, J. Probing Structural and Electronic Properties of the Oxidized $[Fe_4S_4]^{3+}$ Cluster of *Ectothiorhodospira halophila* iso-II High-Potential Iron-Sulfur Protein by ENDOR Spectroscopy. *J. Am. Chem. Soc.* **1999**, *121* (9), 1925−1935.
(46) Hecht, S.; Amslinger, S.; Jauch, J.; Kis, K.; Trentinaglia, V.; Adam, P.; Eisenreich, W.; Bacher, A.; Rohdich, F. Studies on the non-mevalonate isoprenoid biosynthetic pathway. Simple methods for preparation of isotope-labeled (*E*)-1-hydroxy-2-methylbut-2-enyl 4-diphosphate. *Tetrahedron Lett.* **2002**, *43*, 8929−8933.
(47) Woodside, A. B.; Zheng, H.; Poulter, C. D. Trisammonium Geranyl Diphosphate. *Org. Synth.* **1988**, *66*, 211−219.
(48) Gräwert, T.; Span, I.; Bacher, A.; Groll, M. Reductive Dehydroxylation of Allyl Alcohols by IspH Protein. *Angew. Chem., Int. Ed.* **2010**, *49* (47), 8802−8809.
(49) Bradford, M. M. Rapid and sensitive method for the quantitation of microgram quantities of protein utilizing the principle of protein-dye binding. *Anal. Biochem.* **1976**, *72*, 248−254.
(50) Fish, W. W. Rapid colorimetric micromethod for the quantitation of complexed iron in biological sample. *Meth. Enzymol.* **1988**, *158*, 357−364.
(51) Beinert, H.; Albracht, S. P. J. New insights, ideas and unanswered questions concerning iron-sulfur clusters in mitochondria. *Biochim. Biophys. Acta* **1982**, *683*, 245−277.
(52) Hagen, W. R. *Biomolecular EPR Spectroscopy*; CRC Press, 2009. DOI: 10.1201/9781420059588.
(53) Davoust, C. E.; Doan, P. E.; Hoffman, B. M. Q-band pulsed electron spin-echo spectrometer and its application to ENDOR and ESEEM. *J. Magn. Reson. Ser. A* **1996**, *119* (1), 38−44.
(54) Zipse, H.; Artin, E.; Wnuk, S.; Lohman, G. J. S.; Martino, D.; Griffin, R. G.; Kacprzak, S.; Kaupp, M.; Hoffman, B.; Bennati, M.; Stubbe, J.; Lees, N. Structure of the Nucleotide Radical Formed during Reaction of CDP/TTP with the E441Q-$\alpha 2\beta 2$ of *E-coli* Ribonucleotide Reductase. *J. Am. Chem. Soc.* **2009**, *131* (1), 200−211.
(55) Hoffman, B. M.; DeRose, V. J.; Ong, J. L.; Davoust, C. E. Sensitivity Enhancement in Field-Modulated CW ENDOR via RF Bandwidth Broadening. *J. Magn. Reson. Ser. A* **1994**, *110* (1), 52−57.
(56) Davies, E. R. A new pulse endor technique. *Phys. Lett. A* **1974**, *47* (1), 1−2.
(57) Telser, J. Electron-Nuclear Double Resonance (ENDOR) Spectroscopy. In *Applications of Physical Methods to Inorganic and Bioinorganic Chemistry*; Scott, R. A., Ed.; John Wiley & Sons, 2007; pp 99−124.
(58) Hoffman, B. M. ENDOR of metalloenzymes. *Acc. Chem. Res.* **2003**, *36* (7), 522−529.
(59) Doan, P. E. Combining steady-state and dynamic methods for determining absolute signs of hyperfine interactions: Pulsed ENDOR Saturation and Recovery (PESTRE). *J. Magn. Reson.* **2011**, *208* (1), 76−86.

(60) Xiao, Y. L.; Chu, L.; Sanakis, Y.; Liu, P. H. Revisiting the IspH Catalytic System in the Deoxyxylulose Phosphate Pathway: Achieving High Activity. *J. Am. Chem. Soc.* **2009**, *131* (29), 9931−9933.
(61) Hoffman, B. M.; Martinsen, J.; Venters, R. A. General theory of polycrystalline ENDOR patterns. *g* and hyperfine tensors of arbitrary symmetry and relative orientation. *J. Magn. Reson.* **1984**, *59* (1), 110−123.
(62) Huyett, J. E.; Carepo, M.; Pamplona, A.; Franco, R.; Moura, I.; Moura, J. J. G.; Hoffman, B. M. ^{57}Fe Q-band pulsed ENDOR of the hetero-dinuclear site of nickel hydrogenase: Comparison of the NiA, NiB, and NiC states. *J. Am. Chem. Soc.* **1997**, *119* (39), 9291−9292.
(63) Seemann, M.; Janthawornpong, K.; Schweizer, J.; Böttger, L. H.; Janoschka, A.; Ahrens-Botzong, A.; Tambou, M. N.; Rotthaus, O.; Trautwein, A. X.; Rohmer, M.; Schünemann, V. Isoprenoid biosynthesis via the MEP pathway: *In vivo* Mössbauer spectroscopy identifies a $[4Fe\text{-}4S]^{2+}$ center with unusual coordination sphere in the LytB protein. *J. Am. Chem. Soc.* **2009**, *131* (37), 13184−13185.
(64) Ahrens-Botzong, A.; Janthawornpong, K.; Wolny, J. A.; Tambou, E. N.; Rohmer, M.; Krasutsky, S.; Poulter, C. D.; Schünemann, V.; Seemann, M. Biosynthesis of Isoprene Units: Mössbauer Spectroscopy of Substrate and Inhibitor Binding to the [4Fe-4S] Cluster of the LytB/IspH Enzyme. *Angew. Chem., Int. Ed.* **2011**, *50* (50), 11976−11979.
(65) Middleton, P.; Dickson, D. P. E.; Johnson, C. E.; Rush, J. D. Interpretation of the Mössbauer spectra of the four-iron ferredoxin from *Bacillus stearothermophilus*. *Eur. J. Biochem.* **1978**, *88*, 135−141.
(66) Christner, J. A.; Münck, E.; Janick, P. A.; Siegel, L. M. Mössbauer Spectroscopic Studies of *Escherichia coli* Sulfite Reductase - Evidence for Coupling between the Siroheme and Fe_4S_4 Cluster Prosthetic Groups. *J. Biol. Chem.* **1981**, *256* (5), 2098−2101.
(67) Pandelia, M. E.; Lanz, N. D.; Booker, S. J.; Krebs, C. Mössbauer spectroscopy of Fe/S proteins. *Biochim. Biophys. Acta-Mol. Cell Res.* **2015**, *1853* (6), 1395−1405.
(68) Beinert, H.; Holm, R. H.; Münck, E. Iron-sulfur clusters: Nature's modular, multipurpose structures. *Science* **1997**, *277*, 653−659.
(69) Lindahl, P. A.; Day, E. P.; Kent, T. A.; Ormejohnson, W. H.; Münck, E. Mössbauer, EPR, and, Magnetization Studies of the *Azotobacter-Vinelandii* Fe Protein - Evidence for a $[4Fe\text{-}4S]^{1+}$ Cluster with Spin S = 3/2. *J. Biol. Chem.* **1985**, *260* (20), 11160−11173.
(70) Heinnickel, M.; Agalarov, R.; Svensen, N.; Krebs, C.; Golbeck, J. H. Identification of F_X in the heliobacterial reaction center as a [4Fe-4S] cluster with an *S* = 3/2 ground spin state. *Biochemistry* **2006**, *45* (21), 6756−6764.
(71) Duderstadt, R. E.; Brereton, P. S.; Adams, M. W. W.; Johnson, M. K. A pure *S* = 3/2 $[Fe_4S_4]^+$ cluster in the A33Y variant of *Pyrococcus furiosus* ferredoxin. *FEBS Lett.* **1999**, *454* (1−2), 21−26.
(72) Boll, M.; Fuchs, G.; Tilley, G.; Armstrong, F. A.; Lowe, D. J. Unusual spectroscopic and electrochemical properties of the 2[4Fe-4S] ferredoxin of *Thauera aromatica*. *Biochemistry* **2000**, *39* (16), 4929−4938.
(73) Lindahl, P. A.; Gorelick, N. J.; Münck, E.; Orme-Johnson, W. H. EPR and Mössbauer Studies of Nucleotide-Bound Nitrogenase Iron Protein from *Azotobacter vinelandii*. *J. Biol. Chem.* **1987**, *262* (31), 14945−14953.
(74) Bertini, I.; Campos, A. P.; Luchinat, C.; Teixeira, M. A Mössbauer Investigation of Oxidized Fe_4S_4 HiPIP II from *Ectothiorohodospira halophila*. *J. Inorg. Biochem.* **1993**, *52* (3), 227−234.
(75) Middleton, P.; Dickson, D. P. E.; Johnson, C. E.; Rush, J. D. Interpretation of the Mössbauer spectra of the high-potential iron protein from *Chromatium*. *Eur. J. Biochem.* **1980**, *104*, 289−296.
(76) Bominaar, E. L.; Hu, Z.; Münck, E.; Girerd, J.-J.; Borshch, S. A. Double Exchange and Vibronic Coupling in Mixed-Valence Systems. Electronic Structure of Exchange-Coupled Siroheme-$[Fe_4S_4]^{2+}$ Chromophore in Oxidized *E. Coli* Sulfite Reductase. *J. Am. Chem. Soc.* **1995**, *117*, 6976−6989.
(77) Belinsky, M. I. Hyperfine evidence of strong double exchange in multimetallic {$[Fe_4S_4]$-Fe} active center of *Escherichia coli* sulfite reductase. *J. Biol. Inorg. Chem.* **1996**, *1*, 186−188.
(78) Christner, J. A.; Münck, E.; Janick, P. A.; Siegel, L. M. Mössbauer Evidence for Exchange-Coupled Siroheme and [4Fe-4S] Prosthetic Groups in *Escherichia coli* Sulfite Reductase. Studies of the Reduced States and of a Nitrite Turnover Complex. *J. Biol. Chem.* **1983**, *258* (18), 11147−11156.
(79) Moura, I.; Huynh, B. H.; Hausinger, R. P.; Legall, J.; Xavier, A. V.; Münck, E. Mössbauer and EPR Studies of Desulforedoxin from *Desulfovibrio gigas*. *J. Biol. Chem.* **1980**, *255* (6), 2493−2498.
(80) Huynh, B.-H.; Kent, T. A. Mössbauer studies of iron proteins. *Adv. Inorg. Chem.* **1984**, *6*, 163−223.
(81) Münck, E.; Kent, T. A. Structure and magnetism of iron-sulfur clusters in proteins. *Hyperfine Interact.* **1986**, *27*, 161−172.
(82) Yoo, S. J.; Meyer, J.; Achim, C.; Peterson, J.; Hendrich, M. P.; Münck, E. Mössbauer, EPR, and MCD studies of the C9S and C42S variants of *Clostridium pasteurianum* rubredoxin and MDC studies of the wild-type protein. *J. Biol. Inorg. Chem.* **2000**, *5* (4), 475−487.
(83) Xia, J.; Lindahl, P. A. Assembly of an exchange-coupled $[Ni{:}Fe_4S_4]$ cluster in the a metallosubunit of carbon monoxide dehydrogenase from *Clostridium thermoaceticum* with spectroscopic properties and CO-binding ability mimicking those of the acetyl-CoA synthase active site. *J. Am. Chem. Soc.* **1996**, *118*, 483−484.
(84) Weil, J. A.; Bolton, J. R.; Wetrz, J. E. *Electron Paramagnetic Resonance*; Wiley and Sons, 1994.
(85) Carrington, A.; MacLachlan, A. D. *Introduction to Magnetic Resonance with Applications to Chemistry and Chemical Physics*; Harper & Row, 1967.
(86) Ho, M. B.; Jodts, R. J.; Kim, Y.; McSkimming, A.; Suess, D. L. M.; Hoffman, B. M. Characterization by ENDOR Spectroscopy of the Iron-Alkyl Bond in a Synthetic Counterpart of Organometallic Intermediates in Radical SAM Enzymes. *J. Am. Chem. Soc.* **2022**, *144* (38), 17642−17650.
(87) Jodts, R. J.; Wittkop, M.; Ho, M. B.; Broderick, W. E.; Broderick, J. B.; Hoffman, B. M.; Mosquera, M. A. Computational Description of Alkylated Iron-Sulfur Organometallic Clusters. *J. Am. Chem. Soc.* **2023**, *145* (25), 13879−13887.